

NP-11-0027
June 28, 2011

10 CFR 52, Subpart A

U.S. Nuclear Regulatory Commission
ATTN: Document Control Desk
Washington, DC 20555-0001

Subject: Exelon Nuclear Texas Holdings, LLC
Victoria County Station Early Site Permit Application
Response to Request for Additional Information Letter No. 09
NRC Docket No. 52-042

Attached are responses to NRC staff questions included in Request for Additional Information (RAI) Letter No. 09, dated May 6, 2011, related to Early Site Permit Application (ESPA), Part 2, Sections 02.05.01 and 02.05.03. NRC RAI Letter No. 09 contained twenty-three (23) Questions. This submittal comprises a partial response to RAI Letter No. 09, and includes responses to the following eight (8) Questions:

02.05.01-3	02.05.01-10
02.05.01-4	02.05.01-14
02.05.01-7	02.05.01-15
02.05.01-8	02.05.01-16

When a change to the ESPA is indicated by a Question response, the change will be incorporated into the next routine revision of the ESPA, planned for no later than March 31, 2012.

Of the remaining fifteen (15) RAIs associated with RAI Letter No. 09, responses to six (6) Questions were submitted to the NRC in Exelon Letter NP-11-0022, dated June 2, 2011, and responses to six additional (6) Questions were submitted to the NRC in Exelon Letter NP-11-0024, dated June 16, 2011. The response to RAI Question 02.05.01-20 will be provided by July 20, 2011. The response to RAI Questions 02.05.01-5 and 02.05.01-12 will be provided by August 4, 2011. These response times are consistent with the response times described in NRC RAI Letter No. 09, dated May 6, 2011.

Regulatory commitments established in this submittal are identified in Attachment 9.

If any additional information is needed, please contact David J. Distel at (610) 765-5517.

I declare under penalty of perjury that the foregoing is true and correct. Executed on the 28th day of June, 2011.

Respectfully,



Marilyn C. Kray
Vice President, Nuclear Project Development

Attachments:

1. Question 02.05.01-3
2. Question 02.05.01-4
3. Question 02.05.01-7
4. Question 02.05.01-8
5. Question 02.05.01-10
6. Question 02.05.01-14
7. Question 02.05.01-15
8. Question 02.05.01-16
9. Summary of Regulatory Commitments

cc: USNRC, Director, Office of New Reactors/NRLPO (w/Attachments)
USNRC, Project Manager, VCS, Division of New Reactor Licensing (w/Attachments)
USNRC Region IV, Regional Administrator (w/Attachments)

RAI 02.05.01-3:**Question:**

The characterization (nature and extent) of the growth faults that surround and underlie the Victoria County (VC) vicinity, as presented in SSAR section 2.5.1, are based on GeoMap, LiDAR, seismic reflection and air photo data and previously published geologic cross sections. There are inherent and unquantified uncertainties with respect to the precise location of the growth faults as well as with the correlation of faults between the data sets that have not been wholly discussed in the SSAR. For instance, the GeoMap data, in Section 2.5.1.2.4.2.1.2, were interpreted to contain intersections between growth faults and key stratigraphic horizons (only to the top of Frio Formation) derived from borehole data. You also projected fault traces from the Frio Formation to the ground surface. Fault traces at depth are uncertain due to well spacing, and the surface projection adds additional uncertainty. Uncertainties in the Geomap surface traces are not shown on the maps but the SSAR states that uncertainties are “on the order of several miles.”

In addition, there are unqualified uncertainties with the interpretations of surface lineaments (LiDAR and air-photo) that may have been interpreted as fluvial features rather than fault scarps. The figures in the SSAR show a lack of correlation between the traces of LiDAR or air photo lineaments and GeoMap faults for Fault D. The seismic reflection data are petroleum-standard acquisition, therefore these data will not provide resolution of the shallow horizons needed for precise interpretation about the up dip termination of faults so there is uncertainty about where these faults project, and the kind of characteristics that define the end/tip of these faults.

Therefore, in support of 10 CFR 100.23, please provide the following:

1. Please discuss fault location and fault correlation uncertainties with respect to all specific data sets and as an integrated whole.
2. Please provide a figure(s) to reflect the uncertainties (for example, adjusting the line widths).
3. Please discuss how these uncertainties impact your conclusion that no fault projects beneath the power block footprint.

Response:

This RAI question has three parts. Each of these parts is addressed below.

Part 1

As described in the response to RAI question 02.05.01-15, the geologic investigations for the VCS ESP application were conducted following the guidance of NRC Regulatory Guide 1.208 (NRC, 2007). Following from the guidance presented within this document, the investigations focusing on growth faults were conducted at increasing levels of detail as the region of investigation decreased from the 25-mile radius around the site down to the 0.6-mile radius around the site. The investigations conducted as part of the ESPA, and documented in SSAR Subsection 2.5.1.2.4.2, can be summarized as follows.

- Site Vicinity (25-mile radius) investigations – These investigations compiled numerous published (e.g., Dodge and Posey, 1981; Galloway, 1986) and proprietary data sources (e.g., Geomap, 2007) to identify growth faults in the subsurface and used LiDAR data (TNRIS, 2007, 2008) to identify potential growth fault related lineaments (see SSAR Figures 2.5.1-36, 2.5.1-37, and 2.5.1-44).
- Site Area (5-mile radius) investigations – To expand upon the investigations conducted for the site vicinity, several additional data sources were utilized. Detailed geologic mapping was conducted to identify potentially anomalous features (see SSAR Figure 2.5.1-4). Air photos were analyzed to identify potential lineaments related to growth faults (see SSAR Figure 2.5.1-37). Proprietary seismic reflection data was reviewed to identify growth faults within the subsurface and to correlate those faults to potential surface deformation (see SSAR Figures 2.5.1-41, 2.5.1-45, 2.5.1-46, 2.5.1-47, and 2.5.1-48).
- Site (0.6-mile radius) investigations – After identifying growth fault D as the only growth fault associated with potential surface deformation to encroach within the site, additional investigations were conducted to determine whether the potential surface deformation associated with this growth fault impacted the proposed power block area, which it does not (see SSAR Figures 2.5.1-43 and 2.5.1-49).

10 CFR 100.23(d)(2) requires a determination of the potential for surface tectonic and nontectonic deformations and requires that sufficient geological, seismological, and geophysical data be provided to establish whether there is a potential for surface deformation. The goal of the investigations performed at the VCS site, with respect to growth faults, was to identify any growth fault lineaments in the vicinity and, ultimately, determine whether there is any potential for growth faults to cause surface deformation within the power block area. The focus, for the latter, was on the power block area because this boundary delineates the area within which all safety-related structures, systems, and components (SSCs) will be located and was commensurate with the requirements of Criterion 2 of the General Design Criteria (in Appendix A to 10 CFR 50) and Item IV (b) of Appendix S of 10 CFR 50.

In discussing uncertainties associated with growth faults, it is most material to discuss uncertainties associated with growth faults or features that have the potential to impact the power block area (e.g., growth faults close to the power block area or trending towards the power block area from further distances), so the response to this RAI question will focus on the datasets that were used to identify or constrain growth faults within this region of interest (i.e., primarily the seismic reflection and LiDAR data).

The two fundamental datasets used for identifying growth faults, or the absence of growth faults, with the potential to cause surface deformation within the site area are: (a) the seismic reflection data (see SSAR Figures 2.5.1-45 through 2.5.1-48), and (b) the LiDAR data (see SSAR Figures 2.5.1-39 and 2.5.1-41 through 2.5.1-43). The usefulness of these particular datasets for identifying growth faults is expressed in the observations that: (1) there are no growth faults within the Geomap data that intersect the seismic reflection profiles that are not identified within the seismic reflection profiles (as described in SSAR Subsection 2.5.1.2.4.2.3.1.3, growth fault E is an exception to this statement); (2) the only growth fault identified within the seismic reflection as extending above Horizon 3 or 4 (growth fault D) has potentially associated surface deformation independently identified from the LiDAR data (see SSAR Figures 2.5.1-41, 2.5.1-42, and 2.5.1-45 through 2.5.1-48); and (3) the only LiDAR lineament potentially

associated with growth fault surface deformation that is covered by the seismic reflection data (growth fault D) is associated with a shallow growth fault identified within the seismic reflection data (as described in SSAR Subsection 2.5.1.2.4.2.3.1.3, growth fault E is an exception to this statement) (see SSAR Figures 2.5.1-41, 2.5.1-42, and 2.5.1-45 through 2.5.1-48). These observations demonstrate the consistency of the datasets and the ability to correlate faults within the datasets, in particular near the power block area.

The uncertainty associated with the seismic reflection data is discussed in the response to other RAI questions (e.g., 02.05.01-3, 02.05.01-6, 02.05.01-7, 02.05.01-8, 02.05.01-15, 02.05.01-16, and 02.05.01-17). Several of these questions raise the issue of the usefulness of seismic reflection data collected for petroleum exploration purposes (i.e., data optimized to interpret deep structure) in identifying growth faults that may have the potential to cause surface deformation (i.e., the structure of growth faults in the shallow subsurface). This issue of data applicability was identified in the VCS ESPA (see SSAR Subsection 2.5.1.2.4.2.3.1.4), and it was determined that the seismic reflection data presented in the VCS ESPA was adequate for identifying growth faults relevant to the VCS site. One of the justifications for this conclusion is based on the fundamental structure of growth faults within the Gulf coastal plain: growth faults extend from their most updip extent down into detachment surfaces at depth. The implication of this fact is that growth faults are not identified based on their shallow expression (i.e., where data resolution is potentially degraded), but instead they are identified at depth where the data is optimized to resolve structure.

The implications of this observation for the VCS site are that: (1) growth faults at depth are well-located within the seismic reflection data based on using standard of practice data and procedures; and (2) the only potential issue with growth fault locations is at shallow depths where, for faults that extend up to shallow depths (e.g., above Horizon 4), the seismic reflection data may not be able to as clearly resolve continuous reflectors (see SSAR Subsection 2.5.1.2.4.2.3.1.4). However, the potential uncertainty in growth fault locations at these shallow depths does not impact the VCS site because: (1) growth fault D is the only growth fault that extends above Horizon 3 or 4 (see SSAR Figures 2.5.1-45 through 2.5.1-48); (2) the extent of potential surface deformation associated with growth fault D is mapped using LiDAR data as not encroach upon the power block area (see SSAR Figure 2.5.1-43); and (3) the surface projection of the zone of deformation observed at depth does not approach any closer to the site than the zone of surface deformation identified within the LiDAR data (see response to RAI 02.05.01-8).

The location of lineaments identified within the LiDAR data is precise due to the high resolution of the LiDAR topography (see SSAR Subsection 2.5.1.2.4.2.1.4). Therefore, the main issue of uncertainty with respect to growth fault locations and the LiDAR data is whether lineaments identified within the LiDAR data are potentially associated with surface deformation from growth fault activity or other processes (e.g., fluvial origin). The methodology used in the VCS ESPA project for interpreting LiDAR lineaments is described in SSAR Subsection 2.5.1.2.4.2.2, and several responses to other RAI questions discuss specific examples of uncertainty in the interpretation of LiDAR lineaments (e.g., see responses to RAI 02.05.01-9 and 02.05.01-4). Importantly, the only LiDAR lineament (either fluvial or potentially growth fault related) that approaches the power block area is the lineament associated with growth fault D (see SSAR Figures 2.5.1-42 and 2.5.1-43), and for this lineament:

- The zone of potential deformation associated with this lineament has been mapped as not extending to within the power block area (see SSAR Subsection 2.5.1.2.4.2.3.2); and

- The lineament is correlated with a shallow zone of tilting and folding up-dip of growth fault D identified within the seismic reflection data.

Therefore, uncertainty in either the location of lineaments associated with growth faults identified in the LiDAR data or the correlation of the lineaments to growth faults at depth does not have an impact on the conclusions presented within the VCS ESPA regarding the absence of any growth faults with the potential to deform the power block area.

The VCS ESPA also used the Geomap data and lineaments for aerial photographs in the investigation of growth faults. As described in SSAR Subsection 2.5.1.2.4.2, these datasets were used to complement the LiDAR and seismic reflection data, but they were not used as the primary basis for making any conclusions regarding the potential, or lack thereof, for growth faults to cause surface deformation within the power block area. For example, the Geomap data were the first data analyzed for the VCS ESPA that identified the growth faults within the site area. Based on this observation, the effort was undertaken to analyze seismic reflection data within the site area that would better characterize growth faults within the site area. Similarly, aerial photos were used to identify lineaments within the site area, but the aerial photos did not contain any lineaments potentially associated with growth faults that were not identified as such using the LiDAR data. Because both of these data sets were used as compliments to the LiDAR and seismic reflection data, uncertainties inherent in these data do not have an impact on the conclusions regarding the potential for growth faults to cause surface deformation within the power block area.

This RAI question also mentions the published cross sections of Dodge and Posey (1981) and Galloway et al. (1994) that are discussed in the SSAR (see SSAR Subsection 2.5.1.2.4.2.1.1) and that are used to develop growth fault surface projections (see SSAR Figures 2.5.1-36 and 2.5.1-40). These data are referred to within the SSAR to document the review of published information that was conducted as part of the VCS ESPA project, but, as described in 2.5.1.2.4.2.2, these data were not used as the basis for making any conclusions regarding the potential, or lack thereof, for growth faults to cause surface deformation within the power block area. The main reasons these data were not used for this purpose are that:

- The cross sections containing the growth faults are shown with extreme vertical exaggeration (approximately 40-50 times exaggeration), so it is difficult to develop accurate surface projections;
- The intention of the researchers who developed the cross sections was not explicitly to identify the locations of growth faults, so the growth faults are likely not well located; and
- Other subsurface data was available to the project (i.e., seismic reflection data) that could be used to more reliably identify growth faults.

The difficulty in correlating these projections to growth faults identified in other datasets is discussed in SSAR Subsection 2.5.1.2.4.2.2. Thus, based on the reasons described above these datasets were not used to make conclusions regarding the potential for growth faults to cause surface deformation within the power block area.

Part 2

Five datasets are mentioned in this RAI question and discussed in part one of this response. These datasets are the seismic reflection data, the LiDAR data, the Geomap data, the aerial photos, and the published cross sections (see SSAR Subsection 2.5.1.2.4.2). Of these datasets, it is only feasible and appropriate to graphically illustrate the uncertainties in: (1) the Geomap projection locations, (2) the extent of deformation associated with growth fault D observed in the seismic reflection data, and (3) the zone potential surface deformation associated with growth fault D identified using the LiDAR data. The reasons for not graphically illustrating uncertainties with other aspects of these five datasets are summarized as follows.

1. Seismic reflection data – This data is used for two main purposes: (1) identify the location of growth faults in the subsurface, and (2) characterize the deformation associated with growth fault D (the only fault to extend above Horizons 3 and 4) in the shallow subsurface. The locations of growth faults within the subsurface are well defined based on obvious offset of continuous and semi-continuous reflectors. Within the data presented within the SSAR (see SSAR Figures 2.5.1-45 through 2.5.1-48), the interpreted locations of the growth faults are accurate within the width of the lines used to illustrate their location. The uncertainty in the location of subsurface deformation associated with growth fault D is expressed as the gray zone shown in SSAR Figure 2.5.1-48.
2. LiDAR data – As previously discussed in this response, the LiDAR data is of a high resolution (see SSAR Subsection 2.5.1.2.4.2.1.4). Therefore, the lineaments that are identified with the LiDAR data are located to the point where any uncertainty in their position is less than the line width that is used to identify the lineament on the figures within the SSAR (e.g., see SSAR Figures 2.5.1-42 and 2.5.1-44). The only lineament that approaches near the power block area is the lineament associated with growth fault D, and the uncertainty in any potential surface deformation associated with that lineament is expressed in the zone of deformation identified within the SSAR (see SSAR Figure 2.5.1-43).
3. Geomap data – As previously discussed in this RAI response, the Geomap data were also not used to reach any conclusions regarding the presence or absence of growth faults. However, the growth faults identified within the Geomap data are consistent with the growth faults identified in the seismic reflection data, and they provide a good picture of the lateral extent of some growth faults. Therefore, potential uncertainties in the locations of the Geomap projections of faults GM-K, GM-D, and GM-E are discussed below. Only these three faults are discussed because they have the closest projections to the site, and they are the faults that are the focus of RAI questions for SSAR Section 2.5.1.
4. Aerial photos – As previously discussed in this response, the aerial photos were used to identify lineaments. Uncertainty in the location of these lineaments is less than the line width used to indicate their position within the SSAR (see SSAR Figure 2.5.1-37).
5. Published cross sections – As previously discussed in this response, the published cross sections were not used to reach any conclusions regarding the presence or absence of growth faults in the VCS vicinity or site area, so uncertainty in the locations of the projections presented in SSAR Figures 2.5.1-36 and 2.5.1-40 are not discussed in the response to this RAI.

As discussed in SSAR Subsection 2.5.1.2.4.2.1.2, the Geomap data present structural horizon contours of two horizons and the location of growth faults within these horizons. The three-dimensional fault traces from the maps were used to generate the surface projections of growth faults within the site vicinity. The growth fault traces within each horizon were digitized generating three-dimensional traces of the growth faults at each horizon. These traces were used to estimate the dip of the growth fault between the two horizons at each digitized point, and each point was projected from the upper horizon to the surface using the estimate fault dips dip. A smooth, interpreted projection was developed by drawing a line through the cluster of projected points by hand.

The most significant sources of uncertainty in the position of the surface fault projection are derived from: (1) uncertainties in the actual location of the faults at depth, (2) the assumption that the fault dip is constant from the upper horizon to the surface, and (3) the subjective drawing of a smooth line through the projected points of the faults.

It is difficult to evaluate any potential uncertainty in the fault locations at depth within the Geomap data due to the vast amounts of data (both proprietary and publicly available) that were used by the Geomap developers in compiling the maps. However, given the relatively dense well spacing within the site area, in particular surrounding growth faults GM-D and GM-E, it is likely that the growth faults are relatively well located. Therefore, for this analysis the locations of the faults at depth are assumed to be accurate, but it is important to note that the Geomap data were not used to as the primary basis for making conclusions regarding the potential for growth faults to cause surface deformation within the power block area (as discussed above). To estimate any potential uncertainty from drawing a smooth projection, an envelope was drawn surrounding the maximum extent of the projected points (Figure 1).

The uncertainty introduced by the constant dip assumption can be estimated by comparing the projection of the growth faults using the observed dips between the horizons and the maximum possible dip of a growth fault. The median dip determined from the Geomap data for the points along fault GM-D, GM-E, and GM-K are 73°, 68°, and 75°, respectively. Because growth faults are listric, the maximum dip any fault could have above the upper Geomap horizon is 90°. Therefore, the uncertainty in the constant dip assumption is represented by drawing an envelope around the projections that extends from the surface directly above the upper Geomap horizon (i.e., drawn from the upper horizon using a dip of 90°) to the projected surface assuming a constant dip (i.e., drawn from the upper horizon using the observed dips between the two Geomap horizons). These enveloping areas are presented in Figure 1. It should be noted that the projection for growth fault GM-K is purely hypothetical because there is conclusive evidence in the seismic reflection data and LiDAR data that growth fault K does not extend to or deform the surface.

Part 3

The uncertainties associated with the various datasets used to investigate growth faults within the VCS site vicinity do not have an impact of the conclusion that no faults project to the surface within the power block area. This conclusion is based on interpretations of the seismic reflection data, the most accurate representation of the growth fault structure within the site area. These interpretations show that the growth fault that projects the closest to the power block area is growth fault D. As discussed in the response to RAI 02.05.01-10 and in SSAR Subsection 2.5.1.2.4.2.3.2, the subsurface trace of the growth fault correlates with a zone of tilting or folding at the surface, and this zone can be used to define the limits of potential deformation associated

with growth fault D (see SSAR Figure 2.5.1-43). As discussed in part (1) of this response, this zone of deformation takes into uncertainties in the extent of potential surface deformation.

Uncertainties in the various datasets related to the next closest growth fault projection toward the power block area (growth faults E and GM-K) also do not impact the conclusion that the growth faults do not approach the power block area. Surface deformation associated with growth fault E is approximately 2.6 miles from the site and has no potential to extend to the power block area. Growth Fault GM-K is discussed in detail in the response to RAI question 02.05.01-16. This response highlights the conclusion that growth fault GM-K also has no potential to cause deformation within the power block area given: (1) the distance between the surface projection of the fault and the power block area (over 10,000 ft; see Figure 1a of the response to RAI 02.05.01-2); and (2) the absence of any observed deformation of Horizon 3 and above (see SSAR Figures 2.5.1-45 through 2.5.1-47).

It should be noted that uncertainties in the Geomap data indicate that growth fault D may project within the power block area (Figure 1). However, as discussed above the Geomap data are considerably less accurate than the seismic reflection data (for the ability to project faults to the surface) and the LiDAR data (for the ability to identify surface deformation potentially associated with growth faults), which constrain the zone of potential surface deformation associated with growth Fault D to outside of the power block area. Thus, the uncertainties associated with surface projection of the Geomap data do not impact the conclusion that no faults project within the power block area.

Response References:

Dodge, M.M., and Posey, J.S., 1981, Structural cross sections, Tertiary formations, Texas Gulf coast, University of Texas at Austin Bureau of Economic Geology, p. 5, 32 plates

Galloway, W.E., 1986, Growth faults and fault-related structures of prograding terrigenous clastic continental margins: Gulf Coast Association of Geological Societies Transactions, v. 36, p. 121-128.

Galloway, W.E., Liu, X., Travis-Neuberger, D., and Xue, L., 1994, Reference high-resolution correlation cross sections, Paleogene section, Texas coastal plain, University of Texas at Austin Bureau of Economic Geology, p. 19, 5 plates

Geomap, 2007, Upper Texas Gulf Coast Mapping Service maps 327 and 328. Licensed from Geomap Company to William Lettis and Associates, Inc. from February 1, 2007 to January 31, 2008

NRC, 2007, Reg. Guide 1.208: A Performance-Based Approach to Define the Site-Specific Earthquake Ground Motion, US NRC, p. 53

TNRIS, 2007, Meta-data for Victoria, Refugio and Calhoun LiDAR derived elevation datasets, Texas Natural Resources Information Systems (TNRIS)

—, 2008, Summary of Texas Coast LiDAR datasets, Volume 2008, Texas Natural Resources Information Systems (TNRIS), <http://www.tnr.is.state.tx.us/news.aspx?id=724>, accessed on 5-12-2008, <http://www.tnr.is.state.tx.us/news.aspx?id=724>.

Associated ESPA Revision:

No ESPA revision is required as a result of this response.

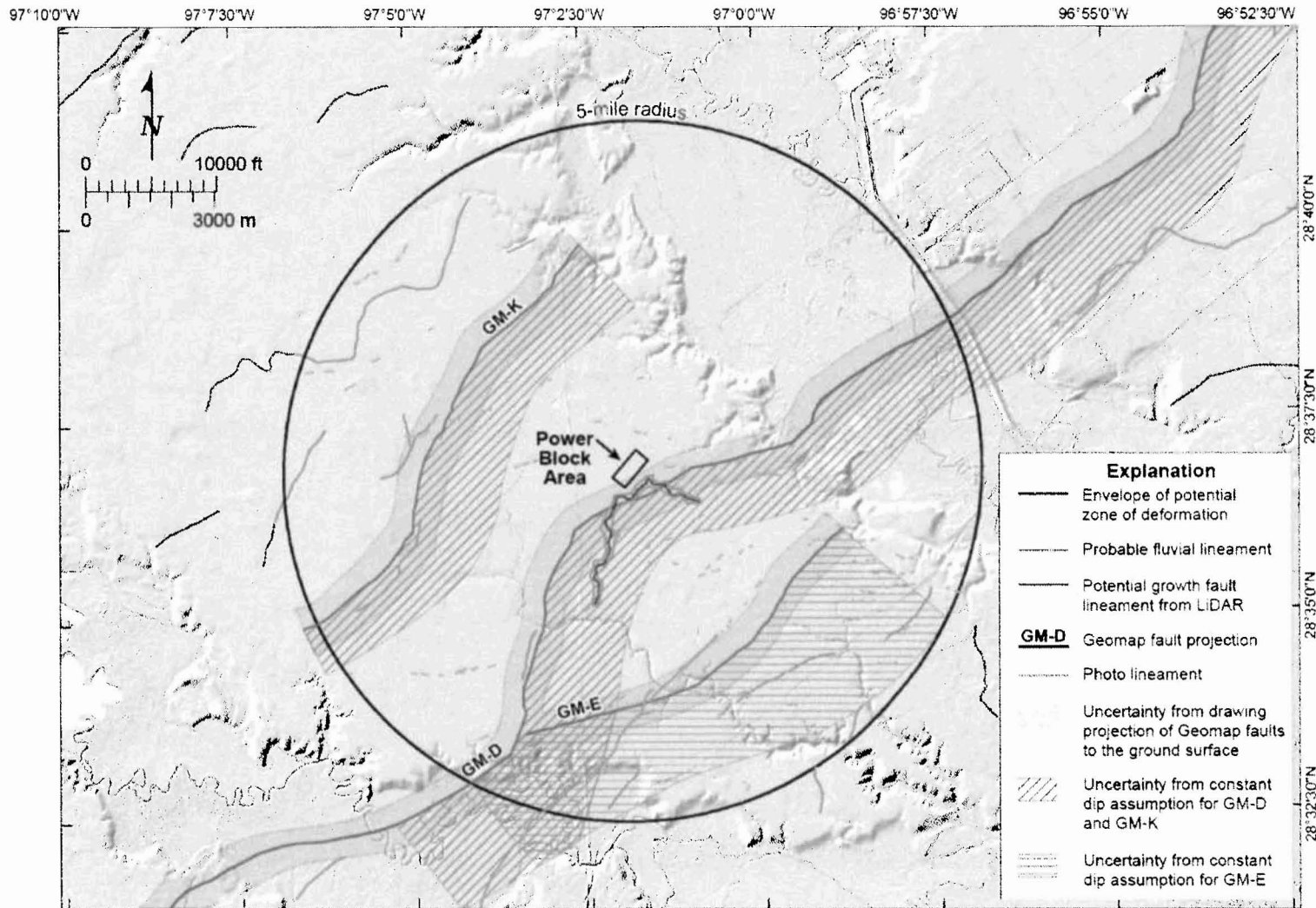


Figure 1. VCS Site Area Map Illustrating Possible Geomap Fault Surface Projection Uncertainty.

RAI 02.05.01-4:**Question:**

SSAR Section 2.5.1.2.4.2.2 describes criteria used to classify lineaments from airphoto and LiDAR data as related either to growth faulting or to non-tectonic processes. Many lineaments interpreted by you to be of fluvial origin (Figs. 2.5.1-37, 41, 42) lie near and on-trend with surface projections of faults K and D (**see attached Figure 1**). One lineament parallels fault K turn-for-turn for more than 3 km, yet is interpreted as fluvial in origin. Many lineaments interpreted as fluvial scarps trend nearly perpendicular to the regional slope and flow direction, and appear to be southeast-facing, consistent with the slip direction of growth faulting in the region. In support of 10 CFR 100.23 please discuss the alternative interpretation that many of these lineaments are surface manifestations of active growth faulting rather than fluvial processes, and the implications for site safety.

Response:

This RAI requests a discussion based on the figure attached to this RAI Letter (titled "*USGS RAI 2.5.1-Figure 1*" and referred to here as NRC Figure 1). Based on the provided caption, the figure represents a composite of Figures 2.5.1-38, 2.5.1-40, and 2.5.1-42 and illustrates the location of several blue lines representing fluvial lineaments (SSAR Figure 2.5.1-42) and green lines representing the surface projection of Geomap growth faults (SSAR Figure 2.5.1-41). The NRC Figure 1 has labeled two of these fluvial lineaments that are the subject of this RAI. The other lineaments shown on NRC Figure 1 are addressed in the response to RAI 02.05.01-9. The fluvial lineaments located adjacent to the surface projection of growth faults GM-K and GM-D are labeled "tectonic? LiDAR lineament parallel to fault GM-K" and "tectonic? LiDAR lineament parallel to fault GM-D," respectively. The discussion below presents the data and observations used to support the designation of these lineaments as fluvial rather than potentially growth fault lineaments.

As described in SSAR Subsection 2.5.1.2.4.2.2, lineaments identified from LiDAR-derived topography and aerial photography were analyzed as part of the VCS ESPA and classified as either potentially related to growth faults or related to fluvial processes (see SSAR Figure 2.5.1-44). The criteria used to make these determinations (described in detail in SSAR Subsection 2.5.1.2.4.2.2) included:

- The degree of linearity and consistency of expression;
- The degree of lateral continuity;
- The presence of cross-cutting relationships; and
- The presence of deflected or otherwise modified fluvial systems.

Using these criteria, and the geologic maps developed as part of the VCS ESP project (see SSAR Figure 2.5.1-5), lineaments identified on aerial photographs and LiDAR were evaluated to determine whether they are potentially related to growth faults or probably related to fluvial process.

As is discussed below, the two lineaments discussed in the RAI request above, although roughly coincident with surface projections of growth faults GM-K and GM-D, do not meet the criteria for growth faults as stated above. Instead, these features consist of subtle tonal and vegetation lineaments that are aligned with localized fluvial features of varying topographic relief. These fluvial features include the inferred margins of geomorphic units and inset stream terraces that have subdued surface expression and are aligned with inferred ancestral surface flow patterns. Figures 1, 2, and 3 were prepared for this RAI response to help illustrate these conclusions. Figure 1 presents a portion of the 5-mile geologic map showing the fluvial lineaments discussed above and surface projections of growth faults GM-D and GM-K. Figures 2 and 3 present six topographic profiles across and parallel to the fluvial lineaments that are the subject of this RAI request.

It is important to clarify that the lineaments shown on SSAR Figure 2.5.1-42 and in the NRC Figure 1 were not necessarily 'interpreted as fluvial scarps' but rather "Probable fluvial lineament(s)" and include features identified on aerial photography. For example, these lineaments coincide in places with inferred topographic features identified on LiDAR but do not consistently have surface expression or lateral continuity that can be attributed to the possible surface expression of growth fault deformation. In addition, although these lineaments locally have a different trend than the regional slope and flow direction, the orientation of the features are consistent with the ancestral flow patterns inferred from subtle paleochannels developed on geologic unit Qbs (Figure 1).

These lineaments that locally coincide with mapped inset fluvial terraces that do not support the interpretation that these lineaments are related to growth faulting (Figure 1). For example, the back edge of geologic unit Qt is coincident with the middle of, and parallel to, the lineament adjacent to the surface projection of growth fault GM-K (see Figure 1). If active growth faulting is occurring across this lineament, it is expected that terrace development and stream incision to have occurred in the inferred area of uplift west of the lineament, not downstream of the lineament in the inferred area of subsidence. Similarly, stream incision and terraces are observed downstream of the lineament that is partially coincident with the surface projection of growth fault GM-D (Figure 1). This observed pattern is the opposite of that expected across the general up-on-the-west displacements of growth faults in the VCS site vicinity. More importantly, the associated fluvial scarps are coincident with other inferred fluvial features identified along the lineaments.

The surface expression of the lineaments in question are not consistent with growth faulting but rather exhibit variable topography derived from surface fluvial processes common within this unit. As discussed in SSAR Subsection 2.5.1.2.4, the Beaumont Formation subunit Qbc consists of levee and flood plain deposits that form locally raised topography that appears as lineaments on LiDAR data and aerial photography. For example, comparison of topographic profiles parallel to, and bracketing, the lineament adjacent to the surface projection of growth fault GM-K illustrates that there is either no change in elevation between the profiles (i.e. no scarp) or that changes in topographic relief are consistent with areas of localized erosion and deposition (Figures 1 and 3). In addition, topographic profiles perpendicular to the lineament coincident with the surface projection of fault GM-K document local absence of topographic relief (scarps) across the lineament (Figure 2). Profiles FF and Y across the lineament coincident with the surface projection of fault GM-D show variable localized changes in topographic relief that are not consistent with large-scale, down-dropping of terrain across a growth fault. In particular, profile FF shows topographic relief consistent with a subdued stream channel. Multiple profiles across the lineament show varying scarps heights generally

increasing towards the existing stream channel to the north, consistent with a fluvial origin.

In conclusion, these lineaments do not meet the criteria used as part of the VCS ESP to identify potential growth fault lineaments (SSAR Subsection 2.5.1.2.4.2.2) because:

- The lineaments do not have consistent topographic expression nor a distinct and consistent linear expression;
- Surface expression across the proposed lineaments, including discrete topographic scarps, is low or non-existent where these lineaments are not associated with inset fluvial terraces or inferred erosional features; and,
- The observed pattern of stream incision and inset fluvial terraces is inconsistent with the inferred sense of offset across faults GM-K and GM-D.

Safety Implications

The proposed NRC lineaments do not have any safety implications to the VCS Site because:

- The lineaments of interest do not appear to have linear topographic expression consistent with lineaments potentially related to growth faults (see discussion above);
- The lineaments are coincident with inferred fluvial features and buried geologic contacts, including inset stream terraces and projected margins of the Qbc geologic unit; and,
- The proposed lineaments do not approach any closer to the power block than the zone of deformation associated with growth fault D (see Figure 1 which shows a 509 ft, 155 m, distance to the power block area and SSAR Figure 2.5.1-43); and the power block area will contain all safety-related systems, structures, and components.

Associated ESPA Revision:

No ESPA revision is required as a result of this response.

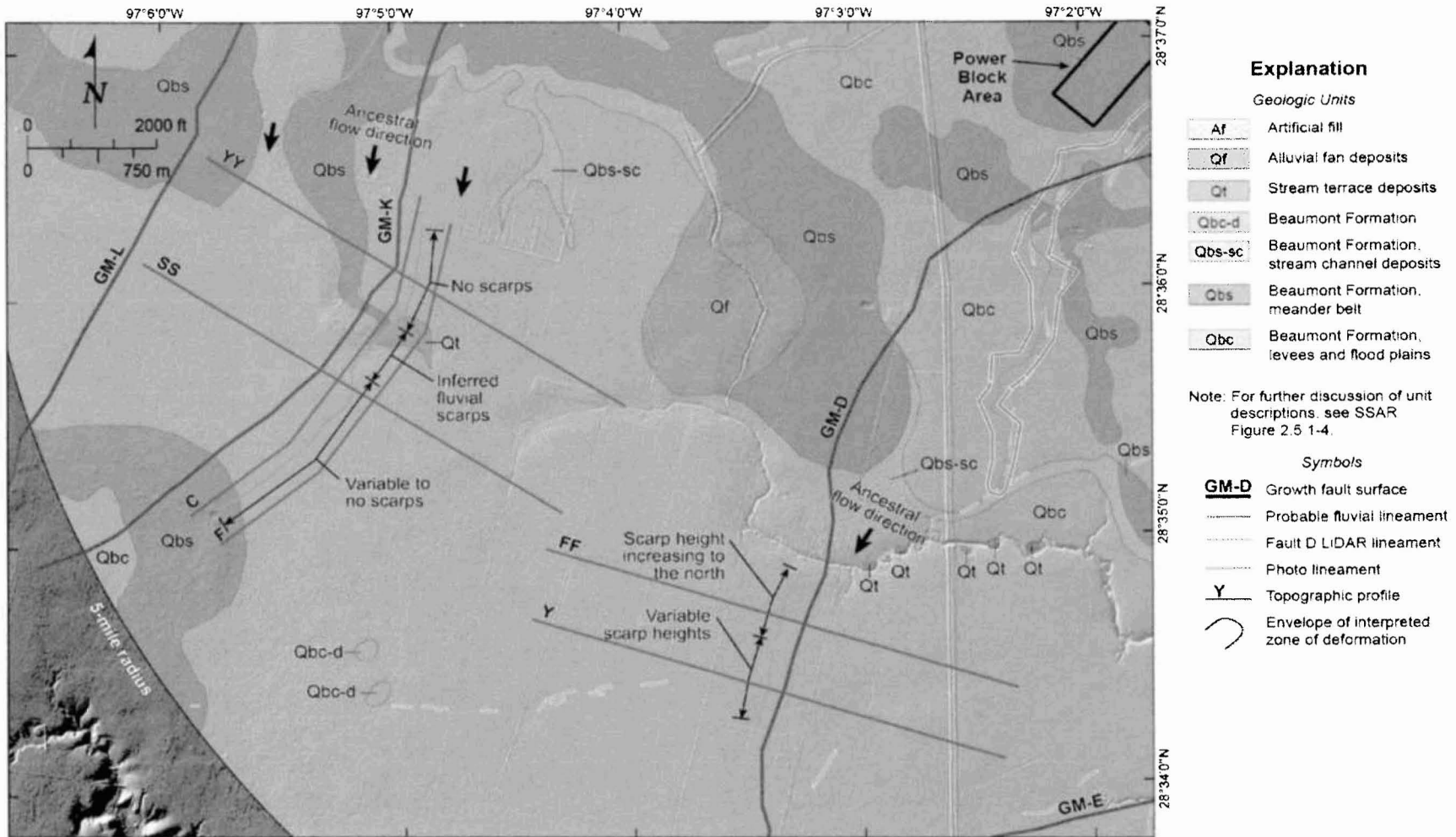
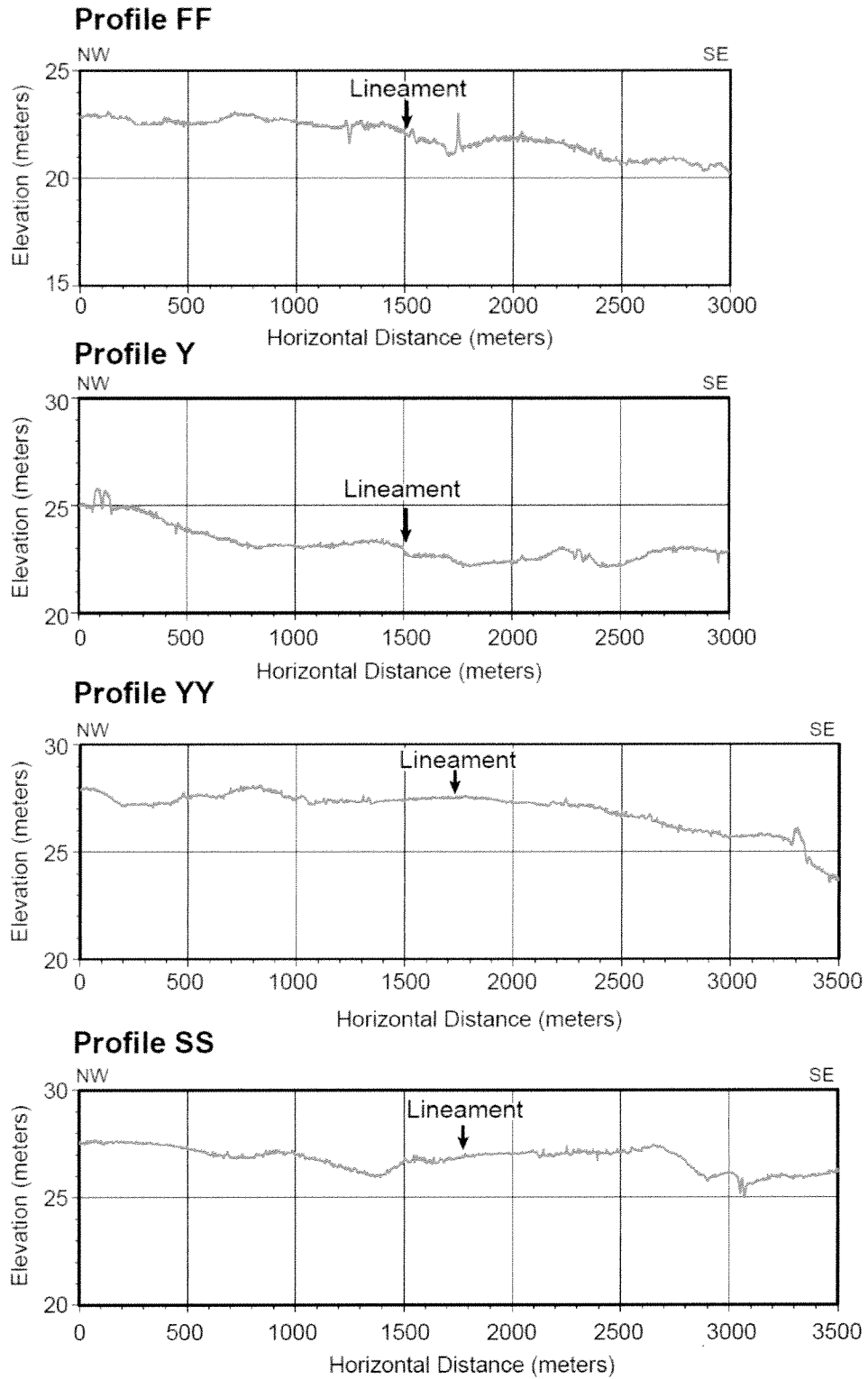
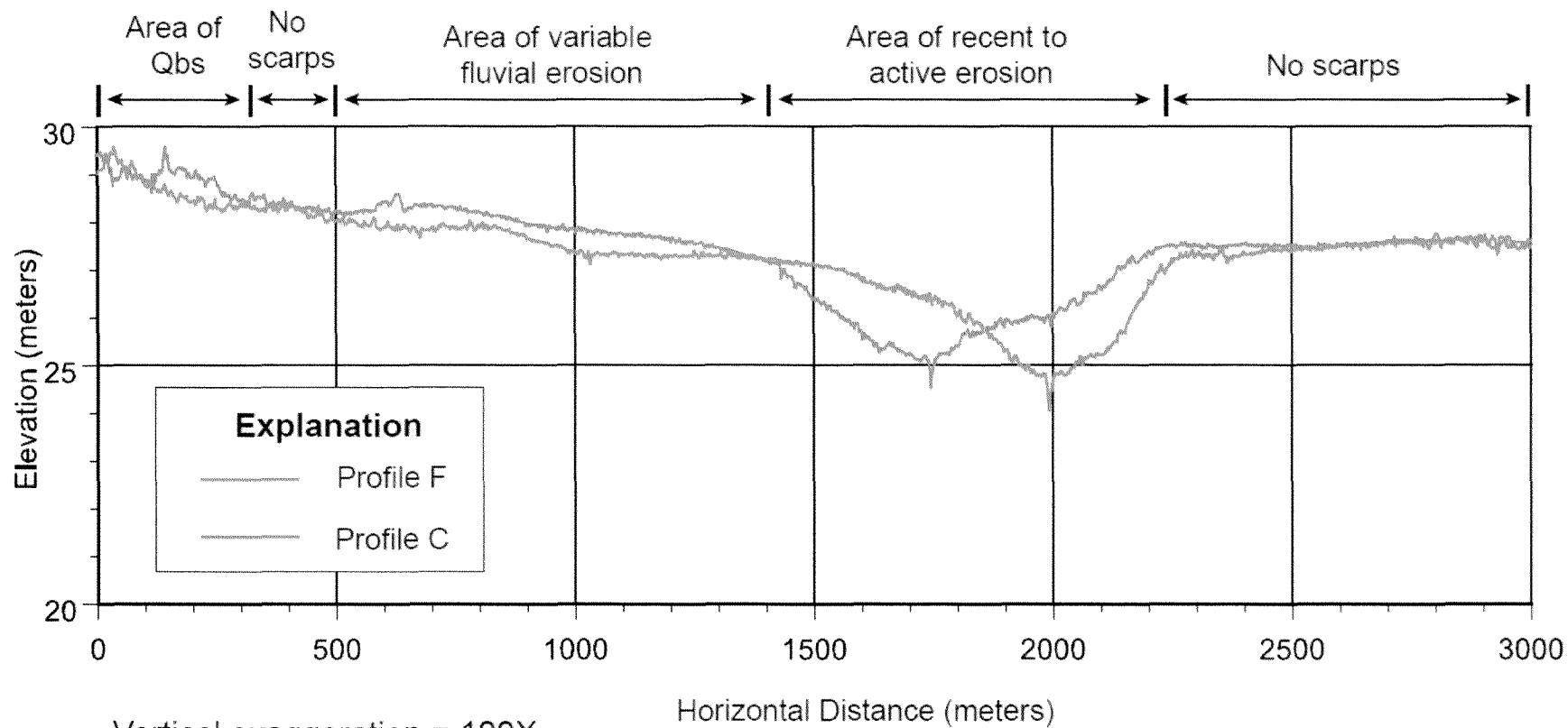


Figure 1 . Geologic Map within the 5-mile Radius.



Vertical exaggeration for all profiles is = 100X
Vertical datum=North American Vertical Datum 1988

Figure 2. Profiles FF, Y, YY, and SS.



Vertical exaggeration = 100X

Vertical datum=North American Vertical Datum 1988

Figure 3. Profiles C and F

RAI 02.05.01-7:**Question:**

The staff notes that velocity fields were developed as part of the data processing for seismic profiles and that each profile crosses at least one other profile. Therefore, the derived velocity fields should be in reasonable agreement where they cross. In accordance with 10 CFR 100.23 (d):

- Provide a discussion on the limitations of this dataset for characterizing growth faults in the VCNPP vicinity
- Describe comparisons of the stacking velocity fields at the profile tie points, and discuss your level of confidence in the interpreted velocity structure
- Describe how sonic log data from deep wells drilled in the vicinity of the VCS site were used in the seismic reflection velocity analysis. For example, were they incorporated directly into the processing or were they compared to the processing-derived velocity field as a quality check?

Response:

As described in SSAR Subsection 2.5.1.2.4.2.3.1.1, Excel Geophysical Services, Inc. (EGS) of Greenwood Village, Colorado, reprocessed all raw seismic reflection data profiles that were obtained from Seismic Exchange, Inc. for the VCS ESP project. EGS performed industry-standard processing of the data to convert the raw seismic reflection data, consisting of arrival times of reflected energy, to 2-D cross sections that display subsurface reflectors in both time and depth domains. To create the depth-domain profiles, EGS performed interactive velocity analyses for each seismic reflection line to develop stacking velocity functions that maximized semblance of supergatherers. The individual velocity functions derived by EGS were compared to existing regional, deep sonic velocity-depth logs compiled for the VCS ESP to qualitatively compare velocities. However, because the closest sonic velocity log is located approximately 18 miles north of the seismic reflection lines, the stacking velocities developed from the independent interactive velocity analyses for each seismic reflection line were deemed most appropriate to use to stack and migrate the data.

For each seismic reflection line, the line's interactive stacking-velocity analyses functions are indexed by Common Depth Point (CDP). Selected CDPs were used as the stacking velocity functions for the line. Figures 1a, b, and c show the stacking velocity functions for the CDPs bracketing the intersection of tie-line PLJ with lines GSI, GDI and TGS. The PLJ-GSI intersection occurs between CDPs 247 and 271 for line PLJ and between CDPs 785 and 799 for GSI (Figure 1a). The PLJ-GDI intersection occurs between CDPs 319 and 343 for line PLJ and between 343 and 365 for line GDI (Figure 1b). The PLJ-TGS intersection occurs between CDPs 364 and 391 on line PLJ and at CDP 5456 for line TGS (Figure 1c). The distance between the bounding velocity functions varies between lines, but is between approximately 0.5 km to 1 km. Figure 1 demonstrates that the stacking velocities are consistent at the intersection points (e.g., tie points), especially above 4 seconds where most of the interpreted structure is mapped (see SSAR Figures 2.5.1-45 through 2.5.1-47).

It should also be noted that during interpretation of the seismic lines, data “mis-ties” were corrected by applying bulk shifts in time or depth. These shifts, based on the locations of prominent reflectors observed on each line, ensured internal consistency of data throughout the seismic array. Profile PLJ was selected as the constant and was not shifted. A time shift of -66 milliseconds (ms) was applied to profiles GSI and GDI. Profile TGS was shifted -30 ms.

Associated ESPA Revision:

No ESPA revision is required as a result of this response.

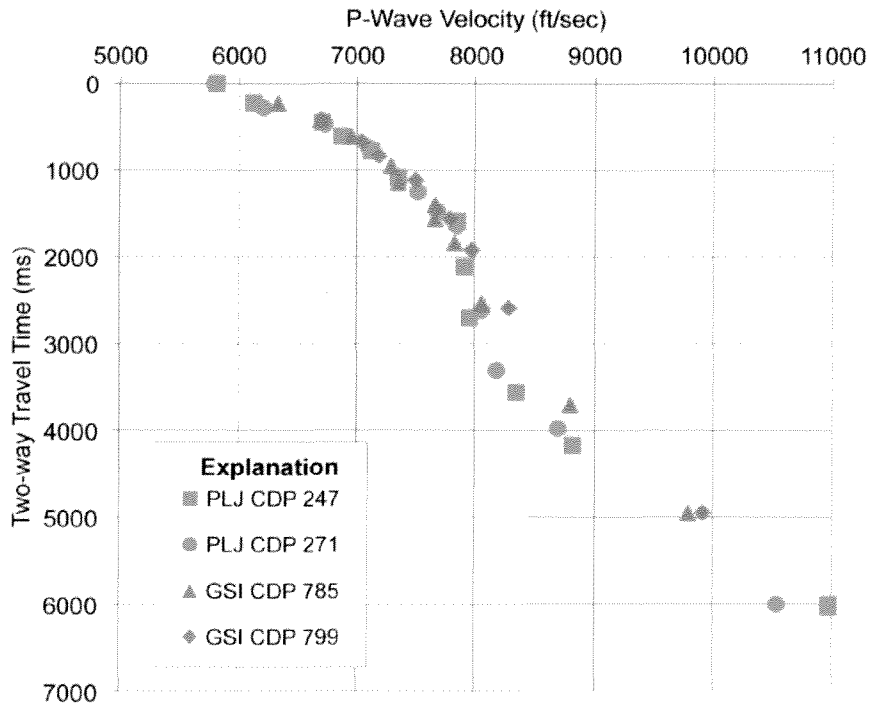


Figure 1a. Stacking Velocities at Intersection of Lines PLJ and GSI.

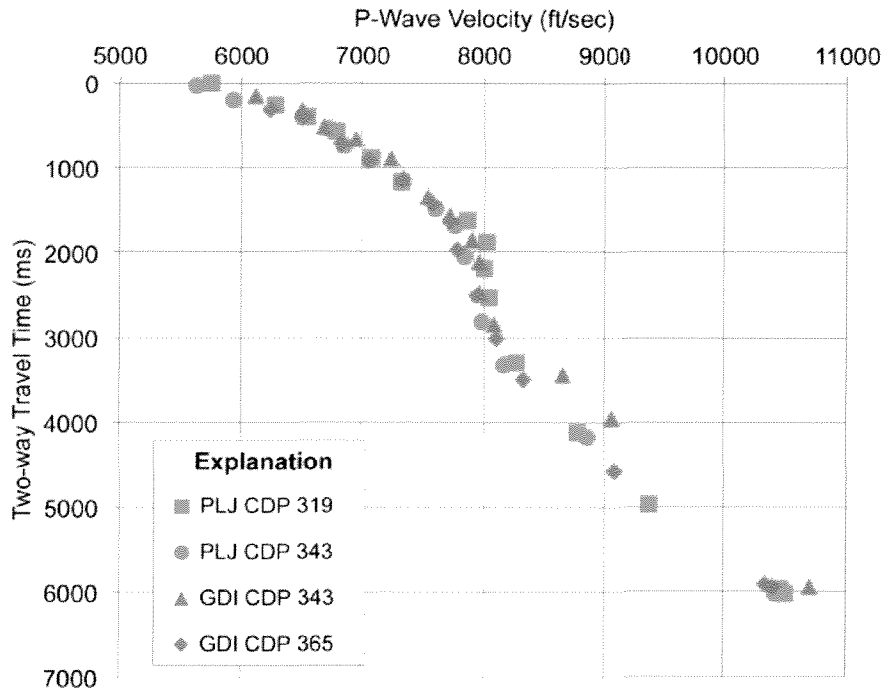


Figure 1b. Stacking Velocities at Intersection of Lines PLJ and GDI.

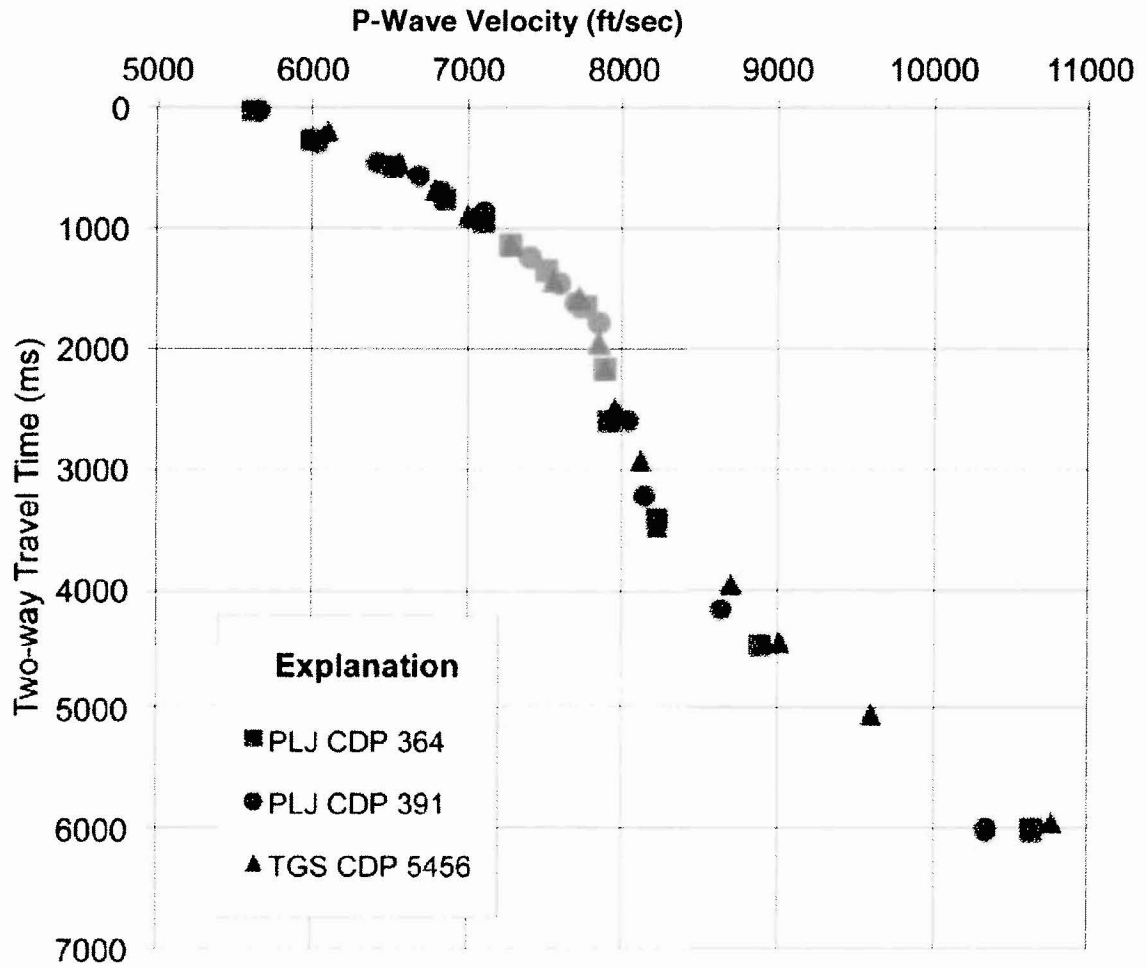


Figure 1c. Stacking Velocities at Intersection of Lines PLJ and TGS.

RAI 02.05.01-8:**Question:**

In SSAR Section 2.5.1.2.4.2.3.1.4, you state that “fault-propagation folding has been observed to occur within triangular zones, called “trishear zones,” updip of the fault tip (Reference 2.5.1-255). The tilting of discontinuous reflectors above Horizon 4 in the shallow subsurface suggests that trishear fault-propagation folding, or some other mechanism of distributed southeast-down tilting, is the primary mode of Quaternary surface deformation related to activity of fault GM-D rather than discrete surface faulting”.

a. In support of 10 CFR 100.23, and to support your conclusion that fault D fault plane does not reach the surface, please provide more details about how you determined that the mode of strain deformation for the shallow expression of fault D was a trishear zone above the tip of the fault plane rather than alternative modes such as simple shear, a single fault plane or even antithetic faulting (2 faults).

Include in your response how you determined the boundary of the zone of deformation based on seismic reflection; how does the fault project up through the triangle zone. If this feature in the seismic reflection data is a trishear zone, how did that determine where you interpreted the location of the fault at the surface and in the shallow subsurface and how does this impact our understanding of the age of latest movement.

b. In response to Question 02.05.01-01, ML 102510229, 8/16/2010, you state that “this style of broad warping is consistent with surface deformation associated with many growth faults throughout the Gulf Coastal Plain.” Please cite and describe published examples of folding of surficial deposits over active growth faults elsewhere in the Gulf Coast region that could support a folding origin for fault D subsurface deformation.

Response:

a) Part (a) of this RAI raises multiple questions regarding growth fault D. Each question is addressed in the following response.

Question 1: Please provide more details about how you determined that the mode of strain deformation for the shallow expression of fault D was a trishear zone above the tip of the fault plane rather than alternative modes such as simple shear, a single fault plane or even antithetic faulting (2 faults).

SSAR Subsections 2.5.1.2.4.2.3.1.4 and 2.5.1.2.4.2.3.2 summarize that the shallow subsurface deformation associated with growth fault D is best characterized by distributed monoclinial fault-propagation folding, possibly through “trishear zones” above the fault tip. The justification for this interpretation is based on: (1) the lack of an apparent discrete fault reflector above horizon 4 (see SSAR Figures 2.5.1-45 through 2.5.1-48), (2) the southeast-down tilting of reflectors in the hanging wall of growth fault D (see SSAR Figure 2.5.1-48), and (3) the spatial correlation of the zone of tilted reflectors with the zone of broad monoclinial tilting or folding observed at the surface (see SSAR Figure 2.5.1-48 and 2.5.1-43).

As described in the last paragraph of SSAR Subsection 2.5.1.2.4.2.3.1.4, trishear fault-propagation was not identified as the mechanism of deformation associated with growth fault D, but it was identified as a possible mechanism for the formation of the distributed tilting observed in the seismic reflection data:

“The tilting of discontinuous reflectors above Horizon 4 in the shallow subsurface suggests that trishear fault-propagation folding, or some other mechanism of distributed southeast-down tilting, is the primary mode of Quaternary surface deformation related to activity of fault GM-D rather than discrete surface faulting.”

The VCS ESP does not propose a single fault plane or antithetic faulting as possible alternate modes of deformation because: (1) the spatial correlation between the zone of tilted reflectors and the surface zone of broad monoclinal folding and (2) the apparent lack of discrete fault offsets above horizon 4 (see SSAR Figure 2.5.1-48 and 2.5.1-43) both support a mechanism of broad tilting or folding. The alternate modes of deformation identified in this RAI question, such as a single fault or antithetic faulting, would most likely produce more discrete zones of deformation and therefore, appear to be inconsistent with a broad zone of deformation observed at the surface.

Question 2: Include in your response how you determined the boundary of the zone of deformation based on seismic reflection?

The zone of deformation identified on the seismic reflection profile shown in SSAR Figure 2.5.1-48 was defined based on the apparent folding and tilting of discontinuous reflectors observed within the seismic reflection data.

Question 3: If this feature in the seismic reflection data is a trishear zone, how does the fault project up through the triangle zone?

As stated in SSAR Subsection 2.5.1.2.4.2.3.1.4, the shallow subsurface deformation associated with growth fault D is interpreted to be fault-propagation folding (SSAR Figure 2.5.1-48). Consistent with this interpretation, SSAR Subsection 2.5.1.2.4.2.3.1.4 also states that a discrete fault plane cannot be identified reaching the surface. However, the zone of distributed deformation shown in SSAR Figure 2.5.1-48 can be projected to the surface, and the northwestern boundary of this zone is approximately coincident with the growth fault D LiDAR lineament (e.g., it does not approach closer to the power block area than the zone of deformation defined from the LiDAR data). The southern margin of the zone of distributed deformation projects to the surface approximately 1,800 ft (549 m) southeast of the envelope of the interpreted zone of deformation.

Question 4: If this feature in the seismic reflection data is a trishear zone, how did that determine where you interpreted the location of the fault at the surface and in the shallow subsurface?

As summarized in SSAR subsection 2.5.1.2.4.2.3.2: (1) the updip projection of growth fault D from the seismic reflection data intersects the ground surface at the topographic lineament associated with growth fault D identified within the LiDAR data; and (2) the zone of deformation updip of the fault D tip, as observed in the reflection data, correlates with anomalous tilting of the land surface (see SSAR Figure 2.5.1-48). These

interpretations were made independent of the possible mode of deformation (trishear or otherwise) in the shallow subsurface.

Question 5: How does this impact our understanding of the age of latest movement?

The mode of deformation associated with growth fault D does not impact the interpretation of the age of latest movement. The age of latest movement is based on the age of the youngest observed deformed deposit, and, as summarized in SSAR Subsection 2.5.1.2.4.2.3.3, the youngest deposit associated with growth fault D deformation is the Beaumont Formation. If the observed deformation was caused by other modes (simple shear, discrete single-plane faulting, discrete antithetic faulting), the observed deformation would still occur in the Beaumont Formation, and the growth fault would have the same age constraint.

Part b. Response

b) Based on the information reviewed for the VCS ESP, the style of broad monoclinial tilting and folding observed at the VCS Site is characteristic of deformation associated with growth faults within this area of the Texas coastal plain. All of the LiDAR lineaments identified within the site vicinity and potentially associated with growth faults (see SSAR Figure 2.5.1-44) have a similar expression. There are no published studies in the peer-reviewed literature compiled as part of the ESPA that discuss the possible near-surface mechanics of growth fault-related deformation in the VCS site vicinity. However, growth faults investigated as part of the South Texas Project (STP) Units 3 & 4 COL application have a similar surface expression (STP, 2007). As part of the STP COL application effort, multiple topographic surveys were conducted across a potential growth fault near the site, and these surveys demonstrated that: (1) there was no apparent discrete faulting at the surface, and (2) surface deformation was best characterized as monoclinial tilting or flexure with approximately several feet of vertical surface elevation change over hundreds of feet (see FSAR Subsection 2.5S.1.2.4.2.2.2 and FSAR Figure 2.5S.1-46 of STP, 2007). The COL application for the STP site concluded that the observed monoclinial tilting or flexure is most likely attributed to fault-propagation folding of the ground surface above the buried tip of growth fault imaged in seismic lines (STP, 2007). Therefore, the STP COL application and the VCS Site ESP make similar observations and reach similar conclusions regarding the surface expression of growth faults and the possible mechanism for broad surface deformation.

References:

STP, *South Texas Project COL application for STP Site, Units 3 & 4, Rev. 5*, NRC Docket Nos. 52-012 and 52-013, accession number ML110340881, 2007.

Associated ESPA Revision:

No ESPA revision is required as a result of this response.

RAI 02.05.01-10:**Question:**

The LiDAR topography profile presented in SSAR Fig. 2.5.1-48, presumably along seismic reflection line GDI, suggests an alternative zone of deformation between horizontal markers at 22,600 ft. and 26,600 ft, which may be a 4000 ft wide graben-like feature. This alternative deformation zone is more than twice as wide as the zone indicated in SSAR Fig. 2.5.1-48 and encompasses the proposed location of Unit 1. LiDAR Profile 8 in SSAR Fig. 2.5.1-50c shows a similar pattern of topographic disruption. In accordance with 10 CFR 100.23 (d),

1. Please explain your justification for defining the boundary of the zone of deformation as the shaded triangle, as interpreted in the Figure 2.5.1-48, rather than the wider zone of deformation postulated above.
2. Please explain how you used the surficial topographic (LiDAR) data to define your interpreted zone of deformation. Also, please explain how the topography could be used to preclude the existence of a wider zone of deformation associated with fault D.
3. Please provide further justification for your interpretation that the lack of a topography break in LiDAR Profile 7 can be attributed to geomorphic or cultural processes rather than a wider zone of deformation between marker 1550 m southeastward to 2400 m, which encompasses the proposed location of Unit 1.

Response:

In the above RAI request, the NRC describes an alternative geometry of the interpreted zone of tilting or folding shown in SSAR Figure 2.5.1-48 and requests: (1) further justification for defining the zone of distributed southeast-tilting or folding interpreted in seismic line GDI shown on SSAR Figure 2.5.1-48; (2) further explanation of how the surficial topographic data were used to define the interpreted zone of deformation with a discussion of how topography can be used to preclude the existence of the wider deformation zone inferred by the NRC request; and (3) provide further justification for geomorphic or cultural process that caused the topographic expression of growth fault D to be muted in Profile 7 (SSAR Figure 2.5.1-50a). A discussion of each request is provided below using the above numbering.

(1) As discussed in SSAR subsection 2.5.1.2.4.2.3.1.4, the interpreted zone of distributed southeast-down tilting or folding shown on SSAR Figures 2.5.1-47 and 2.5.1-48 was determined from the pattern of reflectors in the seismic reflection data above Horizons 3 and 4. Although the seismic reflection acquisition parameters and the nature of the fluvial deltaic deposits within the shallow stratigraphy are not optimal for identifying laterally continuous reflectors above Horizon 4, the interpretation of the seismic reflection data indicate the zone of tilted reflectors does not extend further northwest. As shown on SSAR Figure 2.5.1-48, the zone of tilted reflectors is best resolved at depths of approximately 600 to 800 ft above Horizon 4 by two reflectors between Horizons 3 and 4 (~1400 ft depth). Reflectors northwest of this zone (both above and below) do not exhibit the subtle southeastern tilt as the reflectors within the zone. In summary, the

wider zone of deformation postulated in the RAI request is not supported based on existing interpretations of seismic reflection profile GDI presented in the SSAR.

(2) As discussed in SSAR subsection 2.5.1.2.4.2.3.2, a zone enveloping the interpreted extent of tilting or folding associated with post-Beaumont activity of fault D was developed from analyzing a suite of over 90 LiDAR topographic profiles (SSAR Figure 2.5.1-49). This zone was defined for each profile by identifying the “uphill” and “downhill” extent of deformation. This process included choosing the “top” and “bottom” point defined by identifying the top and bottom of the slope break associated with the zone of deformation. In addition, this process included identifying depositional benching, erosional degradation, and cultural modifications of the land surface that may have masked the zone of deformation (see response to part (3) below for further description and examples from profiles 7 and 8). An envelope was drawn around these points to delimit the maximum extent of interpreted deformation related to post-Beaumont activity of growth fault D. In places where the zone of tilting was significantly degraded, the envelope is dashed, but the potential zone of deformation was drawn well outside of the interpreted extent of growth-fault-related tilting. The few regions of a degraded and possibly muted deformation associated with growth fault D correlate to areas where the growth fault D lineament was poorly defined and to regions of potential erosion or cultural modification.

As stated in the response to issue (a) of RAI question 02.05.01-1, the absence of deformation within the Beaumont Formation in the power block area indicates that there has been no surface deformation of this area since the deposition of the Beaumont Formation between 100,000 to 350,000 years ago. This conclusion is based on the fact that erosional processes are unlikely to have been able to mask or remove all evidence of post-Beaumont deformation (see discussion in the response to RAI 02.05.01-1). The observations of the potential surface deformation associated with growth fault D presented within the SSAR (see SSAR Subsection 2.5.1.2.4.2.3.2) support this conclusion. As described in the SSAR, and in this RAI response, fluvial processes have locally degraded the surface expression of the zone of tilting or folding over a relatively small area. However, these erosional processes have only degraded the surface expression to a limited extent, making the surface deformation appear closer to the power block than it really is over that degraded region. By systematically mapping the zone of interpreted surface deformation across the entire extent of LiDAR lineament, the surface expression of the zone of deformation was readily identifiable in the LiDAR data even within the degraded zones. Therefore, the absence of any surface deformation within the power block area can be used to preclude the existence of a wider zone of deformation associated with fault D.

(3) As summarized as part of section (2) of this response, the zone enveloping the interpreted extent of tilting or folding associated with post-Beaumont activity of growth fault D was developed by analyzing a suite of over 90 LiDAR topographic profiles (SSAR Figure 2.5.1-49) rather than interpreting each topographic profile separately without regard to the overall local geomorphic/cultural setting. Figure 1 was developed to help illustrate the importance of the local setting when interpreting topographic profiles and to help answer the question posed by the NRC above. This figure illustrates the following:

- A color shaded-relief map of LiDAR data around the VCS power block area used to develop topographic profiles discussed in the SSAR text,

- The location of profiles shown on Figures 2.5.1-50a through 2.5.1-50c near the power block area,
- The growth fault D LiDAR Lineament,
- The zone enveloping the interpreted extent of tilting or folding associated with post-Beaumont activity of fault D (the boundary is dashed where surface deformation is interpreted to be degraded), and
- A southeast-flowing drainage (marked by a geomorphically distinct channel) through the power block area.

The color shaded relief map of LiDAR data illustrates several important geomorphic features, including: 1) a southeast-flowing drainage (marked by a geomorphically distinct channel) through the power block area, 2) a series of small topographic bumps along the margins of the channel (suggest the channel has been deepened to improve drainage) and 3) a 'benched' area just south of the zone of deformation subparallel to the axis of the larger drainage (see SSAR subsection 2.5.1.2.4.2.3.2 for a detailed explanation of interpreted 'benched' areas).

As discussed in SSAR subsection 2.5.1.2.4.2.3.2, profile 7 runs through the middle of the southeast-flowing drainage that parallels a broad southeast-sloping topographic low, which has caused erosional degradation of the interpreted zone of deformation associated with growth fault D. In addition, profile 7 is located almost directly coincident with the distinct channel that has been anthropogenically modified near the southeastern and northwestern border of the power block area. The topographic expression of the zone of deformation is more distinct in profile 8, marking the eastern edge of the degraded zone in Figure 1. Likewise, comparison of profiles 7 (degraded) and profile 8 (distinct) suggest that erosion and 'benching' of profile 7 has occurred (see discussion of erosion and benching between profiles 7 and 8 in SSAR subsection 2.5.1.2.4.2.3.2 for further discussion). Thus, the most reasonable explanation of the topographic data is that the broad southeast-trending drainage has caused the muted expression of surface deformation associated with growth fault D along profile 7.

In summary, despite the degradation of the slope break in profile 7, using detailed analysis of the LiDAR data, the zone of potential deformation associated with fault D can be constrained to an area that does not extend to the western portion of the power block area. In particular, the zone of potential deformation along profile 7 is defined based on identifying the characteristic depositional benching and erosional degradation features identified in profiles 2 and 7 (SSAR Figures 2.5.1-50a and 2.5.1-50c).

Associated ESPA Revision:

As a result of this RAI response, it was determined that the labeling of profiles 1 and profile 2 was transposed on SSAR Figure 2.5.1-50a, which resulted in several typographical errors in SSAR Subsection 2.5.1.2.4.2.3.2. SSAR Figure 2.5.1-50a has been revised as part of this response and the revisions to SSAR subsection 2.5.1.2.4.2.3.2 are provided below.

The seventh and eighth paragraphs of SSAR subsection 2.5.1.2.4.2.3.2 shall be revised in a future revision of the ESPA as follows:

It is concluded that the subdued expression of the slope break on profiles 1, 5, and 7 is due to surface run-off that is preferentially captured and directed into the relict Qbs topographic low. Despite the extremely low surface gradients of the tilted surfaces (less than 0.5 degrees), this concentrated ruff-off is preferentially degrading the southeast-facing slope break within the Qbs unit by laying back the tilting of the land surface over a larger horizontal distance. Profiles 1 and 2 provide a clear example of this degradation. Profile 2 runs through the center of the Qbs topographic low, the region of the degraded slope break, and profile 1 runs along the edge of the Qbs and Qbc units in the region expected to have experienced less degradation (Figures 2.5.1-4, 2.5.1-49, 2.5.1-50a through 2.5.1-50c). A comparison of the profiles shows that the profiles have a remarkably similar form with the major difference in topographic shape occurring at the points of highest curvature of the slope break in profile 2. At the highest end of the profile 2 slope break, profile 1 is lower in elevation; at the lowest end of the profile 2, slope break profile 1 is higher in elevation. This relationship between the slope breaks on both profiles suggests that material has been eroded near the “top,” or northwestern end, of the slope break in profile 1 and deposited near the “bottom,” or southeast, end as a “bench” of eroded material. This process effectively decreases the tilting observed in the topographic profile across the slope break. In this example, the cross sectional area of material that has apparently been removed in profile 2 from the uphill end of the slope break is comparable to the cross-sectional area of material apparently added to the downhill end.

Also apparent in profile 1 is a distinct decrease and increase in the topographic profile of approximately 3 feet (1 meter) to the northwest (uphill) of where the power block area projects into the profile. This step in the profile partially masks the tilting of the Beaumont Formation because the relief of the step is on the same order as that of the tilting associated with fault D. From analysis of the LiDAR data, it is apparent that this step reflects modifications of the land surface from a road or pipeline (Figure 2.5.1-49).

Figure 2.5.1-50a will be revised to include the vertical datum, as shown on the attached revised figure.

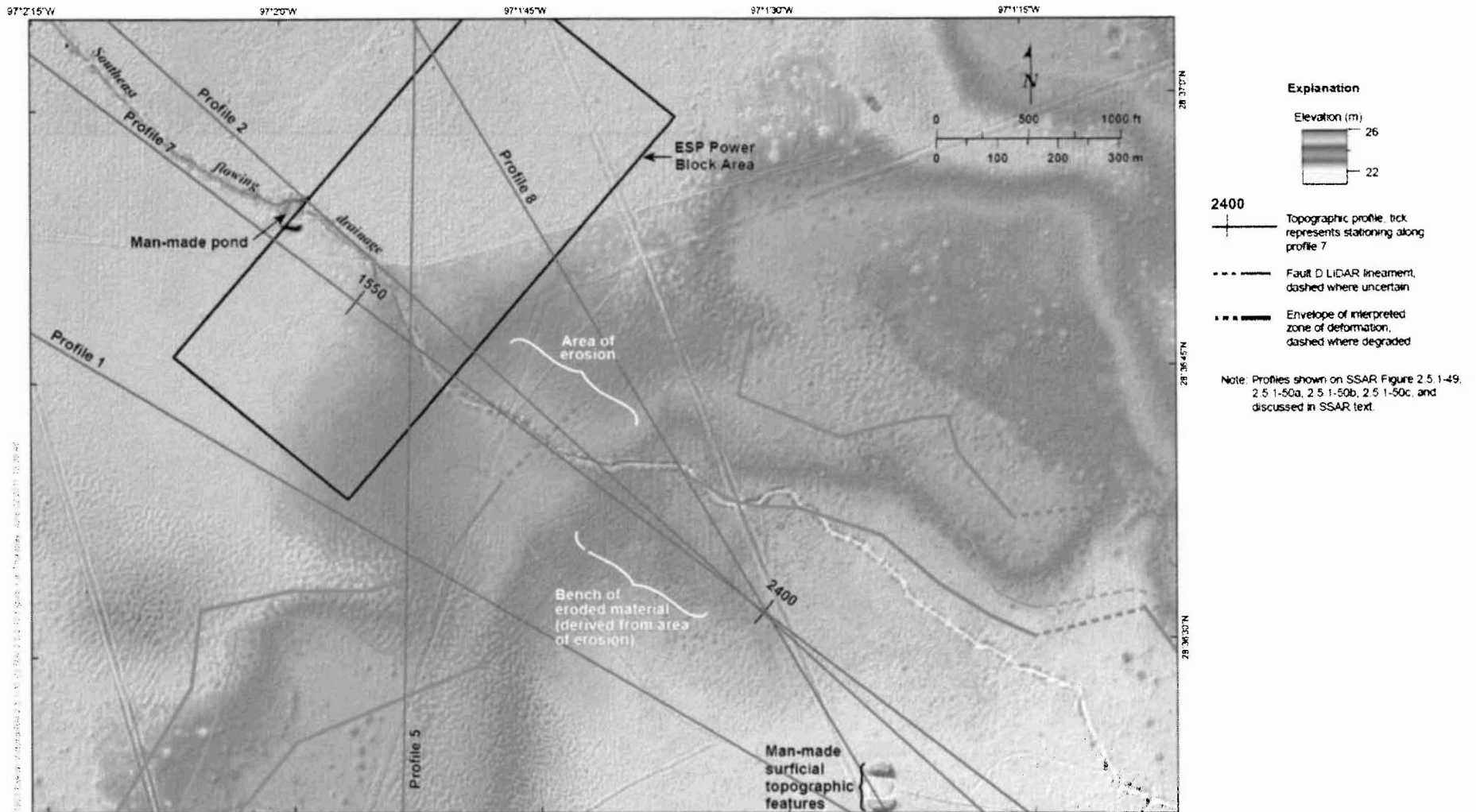


Figure 1. Color Shaded Relief Map of LiDAR Data Adjacent to the VCS Site Showing Location of Topographic Profiles.

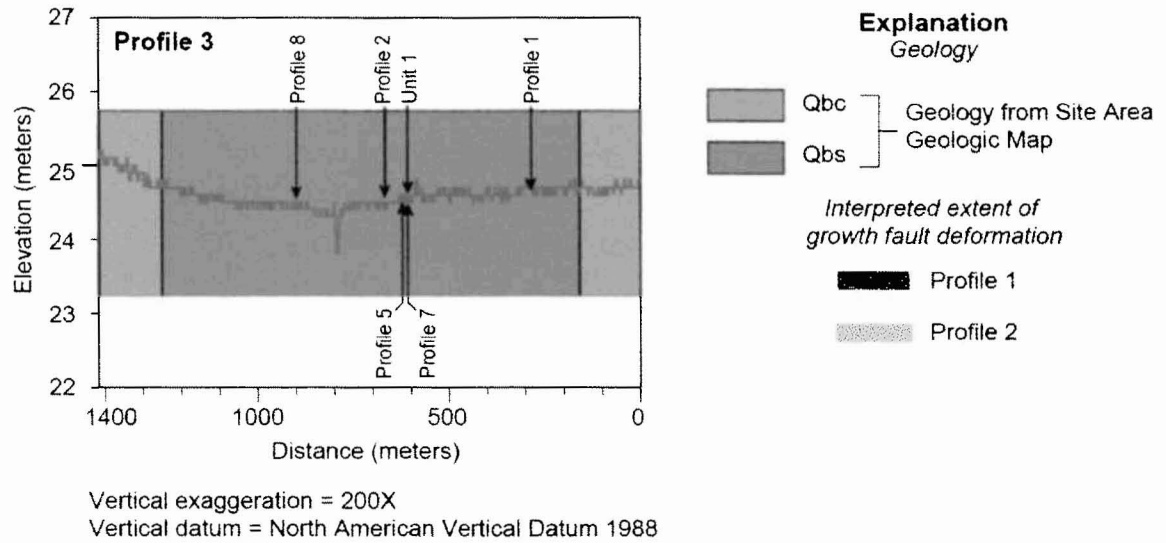
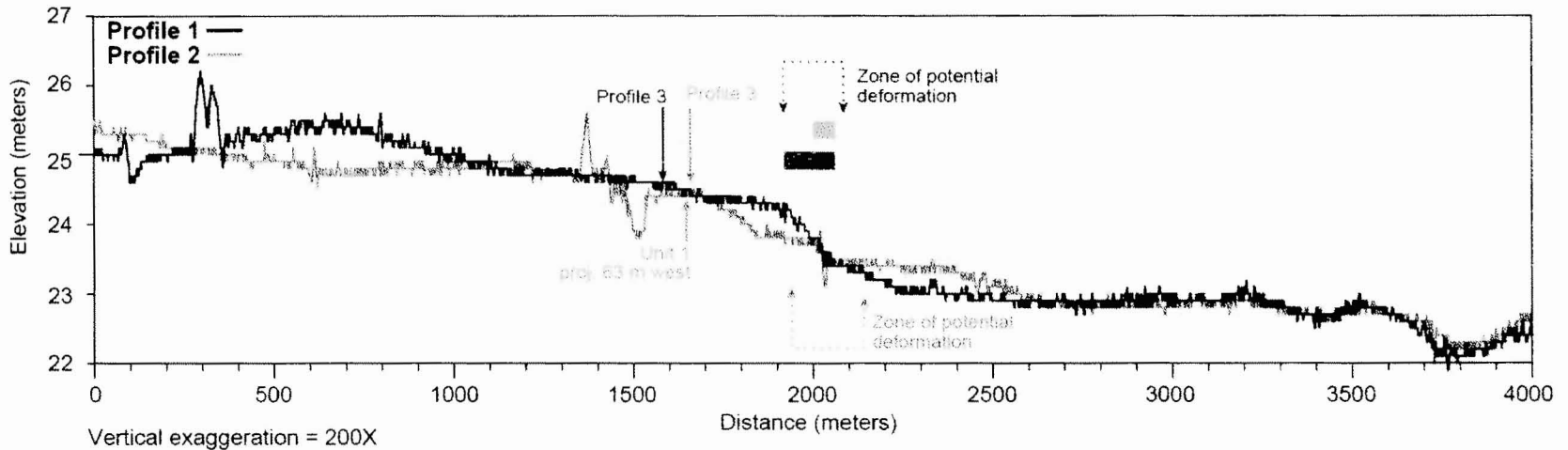


Figure 2.5.1-50a. Fault D Topographic Cross Section (Profiles 1, 2, and 3).

RAI 02.05.01-14:**Question:**

In SSAR Section 2.5.1.1.4.3.4.2 you discuss Tertiary growth faults and state: “However, some faults have either remained active at a much lower rate or have been re-activated as evident in the faults that have extended above the Frio and have minor topographic expressions within Pleistocene units (References 2.5.1-132 and 2.5.1-133)”.

1. In support of 10 CFR 100.23 please discuss alternative explanations for why some growth faults have stopped moving while others remain active (or have been reactivated), and the implications for VCS growth faults. Include a discussion regarding the uncertainty of subsurface faults that may be propagating to the surface.
2. In SSAR Section 2.5.1.2.4.2 you stated that withdrawal of fluid from subsurface strata is a possible mechanism for modern growth fault movement near VC. Please compare withdrawal rates in Victoria County with those in other areas where growth faults have reactivated. If this mechanism is not the causative reason for growth fault reactivation at VCNPP please provide an alternative mechanism.

Response:

This RAI question requests information on two issues related to growth faults near the VCS Site. These two issues are discussed below.

It is important to note that the RAI response below refers to active growth faults as structures that can deform the ground surface, but these faults are not considered capable of producing damaging earthquakes and therefore, are not considered capable seismogenic structures (see SSAR subsection 2.5.1.1.4.3.5.3 and the response to RAI 2.5.3-1 for further discussion).

Part 1

The above RAI requests an alternative explanation for why some growth faults remained active, have become inactive, or have been reactivated. To understand or at least discuss growth fault activity, a review of the mechanisms for growth fault formation and mechanisms associated with reactivation are presented below. The growth faults of the Texas Coastal Plains originally formed due to the gulfward creep and subsidence of associated sediments (Winker, 1982). Growth fault formation is largely driven by 1) compaction and dewatering of the sediment, 2) salt and shale migration, 3) large-scale slumping of the coastal plain due to lateral gradients in gravitational forces, and 4) differential compaction caused by abrupt facies changes (Ewing, 1991; Galloway, et al., 1982; Kreitler, 1976a; Kreitler, 1976b; Morton, et al., 2006; Morton, et al., 2001; Salvador, 1991; Shelton, 1968).

Growth fault reactivation is typically identified based on renewed surface deformation or wetland loss and is largely associated with withdrawal of hydrocarbon and groundwater resources from the subsurface. As discussed in SSAR Subsection 2.5.1.2.4.2, growth

fault reactivation is thought to occur because fluids are commonly trapped within the downthrown side of growth faults and sedimentary compaction from the decrease in pore fluid pressure associated with fluid extraction causes differential subsidence and slip along the growth fault. For example, such activity has been extensively documented around the greater Houston-Galveston area due to large amounts of groundwater and hydrocarbon withdrawal causing damage to infrastructure and buildings (i.e., warped roads and sidewalks, damaged houses) (Kreitler, 1976a; Kreitler, 1976b, 1978; Shah and Lanning-Rush, 2005; Sheets, 1979; Verbeek, 1979; Verbeek, et al., 1979). Surface deformation from reactivated growth fault movement due to fluid withdrawal also has been observed over much of the Gulf Coastal Plains (Alford, 1988; Dubar, et al., 1991; Kreitler, 1976a; Morton, 1985; Morton, et al., 2001; Verbeek, 1979; White and Morton, 1997).

Despite understanding possible causes of reactivation, it is unclear why growth faults D and E have remained active (or at least were active until the Pleistocene) while other growth faults in the VCS Site vicinity have been inactive since late Miocene or Early Pliocene time (SSAR Figures 2.5.1-45, 2.5.1-46, and 2.5.1-47). As discussed in SSAR subsection 2.5.1.2.4.2, inactivity of growth faults is best explained by the cessation of major pulses of deposition and the migration of the paleo-continental shelf away from the VCS site (Winker, 1979).

Based on interpretation of seismic reflection lines, there must be some unknown intrinsic differences between faults D and E and other faults in the VCS Site vicinity that allowed faults D and E to remain active (or at least were active until the Pleistocene). Continued activity on faults D and E (at least pre-historically) may be the result of the same processes that originally created these growth faults (i.e. continued sediment compaction or migration of shale features). Interpretation of both the publically available and proprietary data reviewed as part of the VCS ESPA does not provide any explanation of why growth faults D and E have remained active into at least the Pleistocene, and thus are different than other growth faults in the VCS Site vicinity. Therefore, it is difficult to determine if faults D and E have been active (with a very low slip-rate) since the Pliocene or if they have been reactivated by human activities.

If reactivation is occurring on growth faults in Victoria County, it is expected that only growth fault D would be capable of producing surface deformation near the VCS Site (SSAR Figure 2.5.1-43). Growth faults D and E are the only faults in the site area with associated potential surface deformation and fault E is located too far from the VCS Site (over 2.6 miles, 4.2 km) to affect the site (SSAR subsection 2.5.1.2.4.2.4). There is no research or other available information on the Vicksburg growth faults near the VCS Site that provide evidence that allow for assessment of whether or which faults at depth could propagate to the surface. However, it is most likely that the faults already present in the shallow subsurface with a surface expression (i.e. growth faults D and E) are those that could be potentially reactivated by human activities.

Part 2

Part 2 of the above RAI requests 1) a comparison of withdrawal rates of subsurface fluids in Victoria County to other areas where growth faults have been reactivated and 2) an alternative mechanism for growth fault reactivation if fluid withdrawal is not the causative reason for growth fault reactivation.

The discussion below was developed to address these RAI requests through a discussion of the several studies from the published literature that associate growth fault activity with withdrawal of subsurface fluids and presentation of yearly withdrawal rates of subsurface fluids within Victoria County. However, a meaningful comparison between these studies (Gabrysch, 1982; Holzer and Gabrysch, 1987; Morton, et al., 2006; White and Morton, 1997) and the possible mechanisms for growth fault activity in the VCS Site vicinity is hampered by several factors. There are no reports that document a history of growth fault activity near the VCS Site, so it is difficult to associate fluid extraction with growth fault activity. In addition, compilations of groundwater and hydrocarbon withdrawal rates for Victoria County do not provide a meaningful comparison to extraction values from the published literature because these values represent countywide compilations vs. yearly totals from specific fields. Without these important pieces of information regarding growth fault activity in the vicinity of the VCS Site, trying to establish a mechanism for activity or reactivation is difficult and largely speculative.

Published examples of fault reactivation and withdrawal rates

From the published literature, there are several well-studied examples of potential growth fault reactivation that present compilations of fluid withdrawal (either hydrocarbons or groundwater) and relate these data to surficial growth fault-related deformation. These studies are geographically separated into three groups for ease of discussion: 1) Houston Metropolitan area (Buckley, et al., 2003; Engelkemeir and Khan, 2007; Engelkemeir, et al., 2010; Engelkemeir, et al., 2006; Holzer and Gabrysch, 1987; Kreitler, 1976b, 1978; Sharp, et al., 1991), 2) southeast coastal Texas located southeast of Houston (White and Morton, 1997) and 3) coastal Louisiana (Chan and Zoback, 2007; Morton, et al., 2006).

Houston Metropolitan Area

Within the Houston Metropolitan Area, surface deformation associated with growth faulting is related largely to groundwater withdrawal, but is also related to hydrocarbon withdrawal (Holzer and Gabrysch, 1987). The surface expression and movement of surface faults are well studied using growth fault monitoring stations, GPS Data (Engelkemeir, et al., 2010), LiDAR data (Engelkemeir and Khan, 2007; Engelkemeir, et al., 2006; Engelkemeir and Khan, 2008), and satellite-based interferometry (Buckley, et al., 2003). However, few studies present compilations of yearly withdrawal rates of groundwater and hydrocarbons and compare these to growth fault activity.

Gabrysch (1982) compiled average withdrawal rates of groundwater in the Houston District (including Harris and Galveston counties along with portions of surrounding counties) for a period covering 1975 to 1979. For the entire Houston District, over the period from 1975 to 1979, average daily groundwater withdrawal rates decreased from 505 to 456 million gallons per day (184,325 to 166,440 million gallons per year) resulting in an overall 9.7 percent decrease in water usage. Harris County groundwater withdrawal rates are broken down by area, which indicate that withdrawal rates also decreased from 479 to 438 million gallons per day (174,835 to 159,870 million gallons per year) from 1975 to 1979. However, in the vicinity of the city of Houston, groundwater withdrawal rates increased due to urban expansion from 183.1 to 233.5 million gallons per day (66,831.5 to 85,227.5 million gallons per year) during the same period (Gabrysch, 1982).

Holzer and Gabrysch (1987) use the results of Gabrysch (1982) and other data to relate changes in the water levels from 1977 to 1985 for the upper part of the aquifer beneath Houston and relate these levels to growth fault creep over time. In general, they report that for areas with a net increase in groundwater levels (groundwater recovery) the fault creep rate went down, while for areas where groundwater levels continued to decrease growth fault activity remained somewhat constant. However, Holzer and Gabrysch (1987) report continued slow creep (~1 mm/yr) at several sites of groundwater recovery. They postulate that historical faulting may not be completely related to groundwater withdrawal and that even these low creep rates (~1 mm/yr) do not appear to be representative of the long-term rate over thousands of years because such displacement rates would have produced large prehistoric scarps preserved in the geologic record.

Southeast Coastal Texas

White and Morton (1997) studied wetland losses related to potential growth fault reactivation in southeast coastal Texas. For three oil fields, they identified the potential reactivation of faults using different vintages of aerial photographs to track when growth faults became visible and compared these results with oil and gas production. Two of these fields are discussed below.

In the Port Neches Field, growth faults were not visible until the mid-1960s after the cumulative gas production had reached 40 billion cubic ft (40,000,000 thousand cubic feet or MCF) and oil production had reached approximately 10 million barrels (bbls). Total production in the field produced over 25 million bbls of oil and 40 billion cubic ft of gas between 1929 and 1993 (White and Morton, 1997). While oil production remained somewhat constant between 1929 and 1993 at approximately 390,000 bbls a year, peak gas production occurred between approximately 1955 and 1960 withdrawing approximately 27 billion cubic feet (27,000,000 MCF) of gas, at an average of 5.4 billion cubic ft (5,400,000 MCF) of gas withdrawn each year.

From 1937 to mid-1993, total withdrawals in Clam Lake Field produced 21 million bbls of oil and 4 billion cubic feet of gas (White and Morton, 1997). The approximate average oil and gas withdrawal rate for the Clam Lake Field are 375,000 barrels and 71,000 MCF a year, respectively.

White and Morton (1997) concluded that fault movement was initiated during the first 10 to 20 years of production after 5 million bbls of oil had been extracted from two sites and that fault movement may have been triggered at the Port Neches field by the large volume of gas extraction (~27 billion cubic ft or 27,000,000 MCF).

Coastal Louisiana

Morton et al. (2006) report in coastal Louisiana similar results to White and Morton (1997) by using aerial photo and oil production data to infer possible growth fault reactivation. Morton et al. (2006) present data for Lapeyrouse and Bay Baptiste Field of Louisiana from 1944 to 2002. They present annual data oil withdrawal rates that range from as low as 100,000 bbls and up to as high as 500,000 bbls in 1970, which correlate with peak wetland loss between 1969 and 1974. They also correlate annual formation water withdrawal rates of between 300,000 and 150,000 bbls with wetland-loss between 1987 and 1993.

Chan and Zoback (2007) used an analytical model and numerical modeling of the Lapeyrouse Field in Southern Louisiana to investigate surface subsidence. They conclude that 1) hydrocarbon extraction can cause surface subsidence, 2) all of the measured subsidence cannot be attributed to compaction-induced slip along the principal growth fault at the northern edge of the field, and 3) that land subsidence related to hydrocarbon production is one of several mechanisms that need to be considered when evaluating localized subsidence and wetland loss in Louisiana.

Fluid Withdrawal Rates in Victoria County

Within Victoria County, fluid extraction includes both groundwater withdrawal and fluid extraction related to hydrocarbon production. Yearly groundwater withdrawal rates within Victoria County are compiled as part of the VCS ESPA in SSAR subsection 2.4.12 and shown on SSAR Table 2.4.12-4 titled "Victoria County Historical Water Use". On Table 2.4.12-4, 32 years of records from 1974 to 2006 of water use in the Victoria County are broken down by source (either ground or surface water) and usage (e.g. Municipal, Manufacturing, irrigation etc). Groundwater usage totals reported on Table 2.4.12-4 range from 15,529 to 40,017 acre-feet (5,060 to 13,040 million gallons) between 1974 and 2004.

Within Victoria County, compilations of yearly withdrawal rates of hydrocarbons are available from the Texas Rail Road Commission (TRRC) through their interactive query system (TRRC, 2011). The TRRC provides a summary of hydrocarbon withdrawals per year and separates them into four different types including oil, casinghead (gas produced from an oil well), GW gas (natural gas produced from a gas well), and condensate (liquid gas at atmospheric conditions).

Table 1. Production results from Jan 2001 to Jan 2011 for Victoria County

Date	Oil (BBL)	Casinghead (MCF)	GW Gas (MCF)	Condensate (BBL)
2001	767,273	714,573	29,658,369	325,731
2002	643,123	716,519	23,219,856	214,560
2003	616,914	602,011	22,234,010	197,068
2004	708,436	1,091,022	25,353,391	237,051
2005	653,783	1,001,554	19,820,476	189,339
2006	674,831	813,275	16,200,610	137,483
2007	647,257	878,167	13,808,333	110,088
2008	728,745	720,007	17,142,739	97,124
2009	641,447	799,033	11,707,294	134,793
2010	608,783	732,860	8,410,027	93,521

Source: TRRC 2011

Note: BBL = barrels; MCF = thousand cubic feet.

Casinghead is gas produced from an oil well.

GW Gas: natural gas that is not in contact with an oil reserve

Condensate is liquid gas at atmospheric pressure and temperature.

As shown in Table 1, over the last ten years the overall amount of oil withdrawal within Victoria County ranges between roughly 600,000 to 767,273 barrels and condensate ranges between roughly 100,000 to 325,731 barrels. Casinghead and GW gas range between 600,000 to 1,091,022 thousand cubic feet and 8,410,027 to 29,658,369 thousand cubic feet, respectively (TRRC, 2011). These data summarize hydrocarbon production from multiple oil and gas fields throughout Victoria County.

Comparisons to Victoria County

Below is a comparison between hydrocarbon and groundwater extraction data from the published literature in coastal Louisiana and Texas and estimates from Victoria County. Groundwater extraction data from Victoria County and the Houston Metropolitan area appear to be somewhat similar. For example, between 1974 and 2004 Victoria County groundwater extraction range from 5,060 to 130,396 million gallons per year and in the Houston area groundwater extraction ranged between 160,000 and 185,000 million gallons per year (Gabrysch, 1982).

Oil and gas production in oil fields in Texas and Louisiana that have been associated with growth fault activity are similar to oil and GW gas extraction within Victoria County (Table 1). For example, oil production summarized from fields outside of Victoria County range from 375,000 to 400,000 bbls per year (White and Morton, 1997) to as high as 500,000 bbls per year (Morton, et al., 2006), which is the same order of magnitude as oil extraction within Victoria County (608,783 to 767,273). Gas production from Texas and Louisiana summarized above range from 71,000 to 5,400,000 MCF per year (White and Morton, 1997) (Morton, et al., 2006) and Victoria gas production is similar at (~8,000,000 to 29,000,000 MCF per year). These data suggest that oil and gas production within all of Victoria County is on the same order of magnitude as individual fields in Texas and Louisiana. As discussed above, no published literature compiled as part of the VCS ESPA presented oil and gas extraction data near the VCS site, so a direct comparison to the fields discussed above in Texas and Louisiana is difficult.

Although annual groundwater, oil, and gas production between Victoria County and other areas in Texas and Louisiana appears to be similar in magnitude, it is difficult to compare these values for several reasons, including:

- Published compilations of hydrocarbon production from Texas and Louisiana are from a single field rather than a county-wide compilation of data.
- There are no published studies that associate highly producing oil and gas fields and groundwater withdrawal to growth fault activity in the VCS site.
- It is unclear if the compilations by Morton et al. (2006) and White and Morton (1997) combined the casinghead with GW gas or not.
- There is also no information presented by the Texas RRC (RRC, 2011) documenting the volume or rate of formation water removed or re-injected as part of the hydrocarbon extraction process.

- No published literature compiled as part of the VCS ESPA presented oil and gas extraction data near the VCS site, so a direct comparison to the fields discussed above in Texas and Louisiana is difficult.
- Compiled groundwater data as part of the VCS ESPA (SSAR Table 2.4.12) does not specify the proximity of the groundwater extraction within Victoria County to the VCS site.

Thus, it is unclear if subsurface fluid extraction is the causative reason of growth fault reactivation.

Developing a hypothesis regarding whether or not growth fault reactivation was the result of subsurface fluid extraction (or some other mechanism) is complicated by several factors. First, it is not known whether the growth faults mapped near the VCS site were actively deforming the ground surface before extraction of hydrocarbons and groundwater began. Thus, it is difficult to determine if these faults have been active (with a very low slip-rate) since the Pliocene or if they have been reactivated by human activities. Second, geometrically all of the growth faults appear to be similar in seismic reflection lines (except for growth faults GM-D and GM-E, which extend to the near subsurface and may be active), so there is no obvious structural mechanism that can be identified as a possible cause of continued activity (e.g. a fault that soles into a shale feature while others do not). Third, it is significant that there are no reports that document a history of growth fault activity near the VCS Site since groundwater and hydrocarbon withdrawal began in Victoria County. In the papers reviewed that associate growth fault activity with groundwater or hydrocarbon withdrawal, the authors either note the initiation of growth fault activity (i.e. no growth faults before) or point to a decrease in growth fault creep with the return of groundwater levels (Holzer and Gabrysch, 1987). Without these important pieces of information regarding growth faults in the vicinity of the VCS Site, trying to establish a causal relationship between inactivity, activity or reactivation is difficult and largely speculative.

References:

- Alford, G. W., *Petrology and provenance of the Greta Sandstone, Frio Formation, (Oligocene, McFaddin Field, Victoria County, Texas)* [M.Sc. thesis]: Nacogdoches, TX, Stephen F. Austin State University, 1988.
- Buckley, S. M., Rosen, P. A., Hensley, S. and Tapley, *Land subsidence in Houston, Texas, measured by radar interferometry and constrained by extensometers*: Journal of Geophysical Research, v. 108, p. 8-1 to 8-13, 2003.
- Chan, A. W. and Zoback, M. D., *The Role of Hydrocarbon Production on Land Subsidence and Fault Reactivation in the Louisiana Coastal Zone*: J. Coastal Research, v. 23, p. 771-786, 2007.
- Dubar, J. R., Ewing, T., Lundelius, E. L., Otvos, E. G. and Winker, C. D., *Quaternary Geology of the Gulf of Mexico Coastal Plain*, in Morrison, R. B., ed., *Quaternary Nonglacial Geology: Conterminous U.S., Volume K-2*: Boulder, CA, Geological Society of America, Geology of North America, p. 583-610, 1991.

Engelkemeir, R. and Khan, S., *Near-surface geophysical studies of Houston faults: The Leading Edge*, p. 1004-1008, 2007.

Engelkemeir, R., Khan, S. and Burke, K., *Surface deformation in Houston, Texas using GPS: Tectonophysics*, p. 47-54, 2010.

Engelkemeir, R., Khan, S. and Norman, C., *Mapping active faults in the Houston area using LIDAR*, AAPG Annual Meeting, Houston, TX, , 2006.

Engelkemeir, R. M. and Khan, S. D., *Lidar mapping of faults in Houston, Texas, USA: Geosphere*, v. 4, p. 170-182, 2008.

Ewing, T. E., *Structural framework*, in Salvador, A., ed., *The Geology of North America: the Gulf of Mexico Basin*, Volume J: Boulder, CO, Geological Society of America, p. 31-52, 1991.

Gabrysch, R. K., *Ground-water withdrawals and changes in water levels in the Houston District, Texas, 1975-1979: U.S. Geological Survey Open-File Report 82-431*, p. 45, 1982.

Galloway, W. E., Hobday, D. K. and Magara, K., *Frio Formation of Texas Gulf coastal plain: depositional systems, structural framework, and hydrocarbon distribution: AAPG Bulletin*, v. 66, p. 649-688, 1982.

Holzer, T. and Gabrysch, R., *Effect of water-level recoveries on fault creep, Houston, Texas: Groundwater*, v. 25, p. 392-397, 1987.

Kreitler, C., *Lineations and faults in the Texas coastal zone*, University of Texas at Austin, Bureau of Economic Geology, Report of Investigations No. 85, p. 32, 1976a.

Kreitler, C. W., *Fault Control of Subsidence, Houston-Galveston Area, Texas: Austin, TX, Bureau of Economic Geology, Research Note 5*, p. 17, 1976b.

Kreitler, C. W., *Faulting and Land Subsidence from Ground-Water and Hydrocarbon Production, Houston-Galveston, Texas: Austin, TX, Bureau of Economic Geology, Research Note 8*, p. 22, 1978.

Morton, R. A., *Structural Cross Section, Miocene Series, Texas Continental Shelf: Austin, Texas Bureau of Economic Geology*, p. 8, 1985.

Morton, R. A., Bernier, J. C. and Barras, J. A., *Evidence of regional subsidence and associated interior wetland loss induced by hydrocarbon production, Gulf Coast region, USA: Environmental Geology*, v. 50, p. 261-274, 2006.

Morton, R. A., Purcell, N. A. and Peterson, R. L., *Shallow Stratigraphic Evidence of Subsidence and Faulting Induced by Hydrocarbon Production in Coastal South Texas: Denver, CO, USGS, Open File Report 01-274*, p. 38, 2001.

Salvador, A., *Origin and development of the Gulf of Mexico Basin*, in Salvador, A., ed., *The Gulf of Mexico Basin*, Volume J: Boulder, Geological Society of America, p. 389-444, 1991.

Shah, S. D. and Lanning-Rush, J., *Principal faults in the Houston, Texas metropolitan area*, U.S. Geological Survey, Scientific Investigations Map 2874, 2005.

Sharp, J. M., Jr., Kreitler, C. W. and Lesser, J., *Groundwater*, in Salvador, A., ed., *The Gulf of Mexico Basin*, Volume J: Boulder, Geological Society of America, p. 529-543, 1991.

Sheets, M. M., *Oil Fields, Subsidence and Surface Faulting in the Houston Area*: Houston, TX, Houston Geological Society, Guidebook for 1979 AAPG/SEPM Convention in Houston, TX, p. 23, 1979.

Shelton, J. W., *Role of contemporaneous faulting during basinal subsidence*: AAPG Bulletin, v. 52, p. 399-413, 1968.

TRRC, *RRC Online System - Oil & Gas Data Query*, Texas Railroad Commission, Summary of Oil & Gas Production within Victoria County January 2001 to January 2011, <http://webapps2.rrc.state.tx.us/EWA/productionQueryAction.do>, data downloaded May 23, 2011.

Verbeek, E., R., *Surface faults in the Gulf coastal plain between Victoria and Beaumont, Texas*: Tectonophysics, v. 52, p. 373-375, 1979.

Verbeek, E. R., Ratzlaff, K. W. and Clanton, U. S., *Faults in Parts of North-Central and Western Houston Metropolitan Area, Texas*: Reston, VA, US Geological Survey, Miscellaneous Field Studies Map 1136, 1979.

White, W. A. and Morton, R. A., *Wetland losses related to fault movement and hydrocarbon production, southeastern Texas coast*: J. Coastal Res., v. 13, p. 1305-1320, 1997.

Winker, C. D., *Late Pleistocene Fluvial-Deltaic Deposition: Texas Coastal Plain and Shelf* [MA thesis]: Austin, TX, University of Texas at Austin, 1979.

Winker, C. D., *Cenozoic shelf margins, northwestern Gulf of Mexico*: Transactions-Gulf Coast Association of Geological Societies, v. 32, p. 427-448, 1982.

Associated ESPA Revision:

No ESPA revision is required as a result of this response.

RAI 02.05.01-15:**Question:**

High resolution geophysical studies (Engelkemeir and Khan, 2007, 2008; Saribudak and Van Nieuwenhause, 2006), of active growth faults in the Houston area, which are also a part of the Vicksburg growth fault zone, show shallow distributed zones of shearing and discrete fault planes at very shallow depths beneath surface scarps. They report that rates of movement on these active faults to be as high as 3 cm/year. The faults have caused damage to a variety of man-made structures (buildings, roads, sewer lines, etc.). Fault locations in some cases were unknown until accumulated slip resulted in significant damage. In support of 10 CFR 100.23 and based on the similarity of these growth faults to faults D and E at VCNPP site, please provide the following:

1. Explain why high-resolution techniques were not used to better define the location of potential growth faults at the VC site and to correlate the interpretation from deep seated data sets (seismic reflection and GeoMap) with the topographic breaks interpreted in LiDAR and air photos.
2. Discuss why the Houston area Vicksburg growth faults should not be consider to be an analog for VC vicinity growth faults.
3. Discuss how uncertainties with respect to fault location and fault activity may impact your evaluation of surface fault hazards.

Engelkemeir and Khan, The Leading Edge, August 2007, p. 1004-1008

Engelkemeir and Khan, Lidar mapping of faults in Houston, Texas, USA. Geosphere, 2008, v. 4, no 1 p. 170-182.

Saribudak and Van Nieuwenhause, The Leading Edge, March, 2006, p. 332-334.

Response:

This RAI question requests information on three separate issues. Each of these issues is discussed below.

Issue 1

The geologic investigations for the VCS ESP application (ESPA) were conducted following the guidance of NRC Regulatory Guide 1.208 (NRC, 2007). Following from the guidance presented within this document, the investigations focusing on growth faults were conducted at increasing levels of detail as the region of investigation decreased from the 25-mile radius around the site down to the 0.6-mile radius around the site. The investigations conducted as part of the ESPA, and documented in SSAR Subsection 2.5.1.2.4.2, can be summarized as follows.

- Site Vicinity (25-mile radius) investigations – These investigations compiled numerous published (e.g., Dodge and Posey, 1981; Galloway, 1986) and proprietary data sources (e.g., Geomap, 2007) to identify growth faults in the

subsurface and used LiDAR data (TNRIS, 2007, 2008) to identify potential growth fault related lineaments (see SSAR Figures 2.5.1-36, 2.5.1-37, and 2.5.1-44).

- Site Area (5-mile radius) investigations – To expand upon the investigations conducted for the site vicinity, several additional data sources were utilized. Detailed geologic mapping was conducted to identify potentially anomalous geomorphic features (see SSAR Figure 2.5.1-4). Air photos were analyzed to identify potential tonal and vegetation lineaments related to growth faults (see SSAR Figure 2.5.1-37). Proprietary seismic reflection data were reviewed to identify growth faults within the subsurface and to correlate those faults to potential surface deformation (see SSAR Figures 2.5.1-41, 2.5.1-45, 2.5.1-46, 2.5.1-47, and 2.5.1-48).
- Site (0.6-mile radius) investigations – After identifying growth fault D as the only growth fault associated with potential surface deformation to encroach within the site, additional investigations were conducted to determine whether the potential surface deformation associated with this growth fault impacted the proposed power block area, which it does not (see SSAR Figure 2.5.1-49).

As detailed in this summary, high-resolution techniques were used to define the location of potential growth faults. Similar to the references cited in this RAI question (e.g., Engelkemeir and Khan, 2007, 2008), high-resolution, LiDAR-derived topographic data were used to identify potential lineaments related to growth faults (see SSAR Subsection 2.5.1.2.4.2.1.4 and SSAR Figure 2.5.1-44 and 2.5.1-42). The LiDAR topographic data also were used to map in detail the possible extent of deformation related to growth fault D (see SSAR Figure 2.5.1-43). Additional datasets were not collected to refine the correlation between growth faults observed at depth in either the seismic reflection data or Geomap data because:

- Growth fault D is the only fault with any evidence of post Early Pliocene displacement with the potential to impact structures within the 0.6-mile radius (see SSAR Subsection 2.5.1.2.4.2.3.1.4);
- The seismic reflection data image a clear relationship between growth fault D and the LiDAR lineament directly south of the power block (see SSAR Figure 2.5.1-48 and SSAR Subsection 2.5.1.2.4.2.3.2); and
- The detailed LiDAR mapping demonstrates that potential deformation associated with the growth fault D lineament does not extend to within the power block area (see SSAR Figure 2.5.1-43).

In summary, other investigative methods, including subsurface geophysical exploration (Sariabudak and Van Nieuwenhuise, 2006), were not conducted as part of the VCS ESPA because the efforts presented within the ESPA, and summarized above, are sufficient to demonstrate that: (1) no growth faults project to the surface within the power block area; and (2) the closest approach of potential deformation to the power block area, associated with a growth fault, is no closer than approximately 509 feet (155 m). Particular attention was paid to the power block area because it includes the area within which all safety-related structures, systems, and components (SSCs) will be located.

Issue 2

The VCS ESPA makes no statements that the Houston area Vicksburg growth faults should or should not be considered analogs to the growth faults within the site vicinity. The SSAR does state that there is documentation of fluid extraction leading to apparent growth fault movement within the greater Houston-Galveston area (see SSAR Subsection 2.5.1.2.4.2). However, no such reports of this type of behavior within the VCS site vicinity have been identified during or since the preparation of the VCS ESPA (see response to RAI 02.05.01-14).

Regardless of whether or not the growth faults near the VCS site are analogous to Houston area Vicksburg growth faults, no growth faults project to the surface within the power block area and the closest approach of potential deformation, associated with growth fault D, to the power block area is approximately 509 feet (155 m). Thus, any potential future movement of growth fault D would not have an impact on nuclear safety (see response to RAI 02.05.01-20).

Issue 3

The discussion of surface fault hazards for the VCS ESPA focuses on potential hazards within the power block area because it defines the area within which all safety-related SSCs will be located. Therefore, the response to this RAI addresses the implications of uncertainty in fault locations and activity with respect to growth faults that could intersect the power block area. Growth fault D is the closest identified growth fault to the power block, so it is discussed below. Based on the seismic reflection data (see SSAR Figure 2.5.1-47) and the Geomap data (see SSAR Figure 2.5.1-41), no other growth faults are projected within the site 0.6-mile radius.

Of the faults identified at depth, the growth faults that project the next closest to the power block are the two splays of SR-04 (see SSAR Figure 2.5.1-48; note that this figure is in the time domain, as opposed to depth, so it cannot be used to accurately project the fault to the surface). SR-04 only extends to depths as shallow as approximately 6000 feet (see SSAR Figure 2.5.1-4), so there is some uncertainty in where the projection of the fault beyond its termination would intersect the surface. However, the uncertainty in the projections of the two splays does not impact the evaluation of surface fault hazards because: (1) the seismic reflection data show evidence for no post Early Pliocene deformation from SR-04 along reflection line GSI, which is west of the site (see Figure 1 of the response to RAI 02.05.01-2 for a location map of the reflection lines); (2) the seismic reflection data show evidence of no post-Vicksburg deformation from SR-04 along reflection line GDI, which crosses through the power block area (see Figure 1 of the response to RAI 02.05.01-2 for a location map of the reflection lines); and (3) there are no anomalous geomorphic features indicative of surface deformation at any of the possible locations these growth faults would project to.

As discussed in this RAI response, growth fault D is the only growth fault with associated surface deformation within the site (0.6-mile radius), and the potential deformation associated with this fault is identified as a zone approaching no closer than 509 feet (155 m) to the power block. This estimate, because it comes from defining a "zone of potential surface deformation", includes uncertainty in the exact position of the surface trace of the fault. Therefore, uncertainty in the location of growth fault D is accounted for in the evaluation of surface fault hazards.

Response References:

- Dodge, M. M. and Posey, J. S., *Structural cross sections, Tertiary formations, Texas Gulf coast*, University of Texas at Austin Bureau of Economic Geology, p. 5, 32 plates, 1981.
- Engelkemeir, R. M. and Khan, S. D., *Near-surface geophysical studies of Houston faults: The Leading Edge*, v. 26, p. 170-182, 2007.
- Engelkemeir, R. M. and Khan, S. D., *Lidar mapping of faults in Houston, Texas, USA: Geosphere*, v. 4, p. 170-182, 2008.
- Galloway, W. E., *Growth faults and fault-related structures of prograding terrigenous clastic continental margins: Gulf Coast Association of Geological Societies Transactions*, v. 36, p. 121-128, 1986.
- Geomap, *Upper Texas Gulf Coast Mapping Service maps 327 and 328. Licensed from Geomap Company to William Lettis and Associates, Inc. from February 1, 2007 to January 31, 2008.*, 2007.
- NRC, *Reg. Guide 1.208: A Performance-Based Approach to Define the Site-Specific Earthquake Ground Motion*, US NRC, p. 53, 2007.
- Sariabudak, M. and Van Nieuwenhuise, B., *Integrated geophysical studies over an active growth fault in Houston* The Leading Edge, v. 25, p. 332-334, 2006.
- TNRIS, *Meta-data for Victoria, Refugio and Calhoun LiDAR derived elevation datasets*, Texas Natural Resources Information Systems (TNRIS), 2007.
- TNRIS, *Summary of Texas Coast LiDAR datasets*, Texas Natural Resources Information Systems (TNRIS), <http://www.tnris.state.tx.us/news.aspx?id=724>, accessed on 5-12-2008, <http://www.tnris.state.tx.us/news.aspx?id=724>, data downloaded 5-12-2008, 2008.

Associated ESPA Revision:

No ESPA revision is required as a result of this response.

RAI 02.05.01-16:**Question:**

In SSAR Section 2.5.1.2.4.2.3.1.4 you describe growth fault stratigraphic and structural relationships and state that in seismic reflection data “Horizon 3 is undeformed above fault K, demonstrating the absence of activity since Early Pliocene time.”

The staff notes that in the original GDI profile, two mute zones between about shot points 245 and 251 correspond to acquisition undershoots, areas the seismic field crew could not access (seismic observer logs, supplemental seismic reflection data). Fault K may project to the surface in the region of these mute zones, implying that the power block may be located on the hanging wall of this growth fault. In addition, with minor changes to the interpretation there is evidence to suggest offset of horizons H3 and H4 in this shot point range. In support of 10 CFR 100.23, please address the following:

- a. Discuss the potential for Fault K to propagate to the surface and in particular whether the unmigrated seismic data were analyzed in determining if Fault K cuts through the H3 and H4 horizons.
- b. Discuss your interpretation of Fault K deformation in light of its potential proximity to the power block.

Response:

a. As described in this RAI question, on seismic reflection line GDI growth fault GM-K (referred to as Fault K in the RAI question above) projects to the surface near two muted zones of the reflection data that do not have observable reflector horizons. These muted zones extend down to horizon 4. Based on the time-migrated seismic reflection lines, GM-K appears to project to these muted zones and, based on the depth-migrated seismic reflection line, GM-K projects to or just north of the muted zones.

Regardless of the exact location of the surface projection of GM-K relative to the muted zones, the seismic reflection data support the conclusion of the VCS ESPA that growth fault GM-K has evidence of no deformation of horizons 3 and 4. This conclusion is based on interpretations of the seismic data that show:

- Horizon 3 or 4 are not offset up-dip of GM-K on seismic line GDI;
- There is no convincing evidence of offsets in the relatively continuous reflectors above the tip of GM-K in line GDI and below horizon 3 (i.e., even if the NRC’s alternate interpretation of horizon 3 and 4 suggests deformation of those horizons, deeper horizons do not appear to support the interpretation of growth fault GM-K extending to horizon 3); and
- Lines GSI and TGS, which are close to line GDI where GM-K would project to the surface (see Figure 1a of the response to RAI 02.05.01-2), do not have the same muted zones above GM-K, and there is no convincing evidence of offsets in horizon 3 and 4 from GM-K on these lines.

The unmigrated data were reviewed as part of the VCS ESPA project, but the interpretations of growth fault structure were primarily based on the time- and depth-migrated data. In response to this RAI question, the unmigrated data for GDI were reviewed again. The unmigrated data show horizon 3 above growth fault GM-K, but horizon 4 in the unmigrated data are less well resolved. Interpretation of this unmigrated seismic line suggests that there is no deformation of horizon 3 and, therefore, supports the conclusions presented in this RAI response that there is evidence that GM-K does not deform horizon 3.

b. Within the VCS ESPA, growth fault GM-K is interpreted as not extending shallower than a depth of approximately 3000 ft (see SSAR Table 2.5.1-4), and it is observed that there is no surface deformation in the proximity of the surface projections of the growth fault (see SSAR Figure 2.5.1-42). At its closest approach, the surface projection of growth fault GM-K is located over 13,000 ft (3,900 m) northwest of the power block area based on the Geomap data and over 11,000 ft (3,350 m) northwest of the power block area based on the seismic reflection data (see Figure 1a of the response to RAI 02.05.01-2). As discussed in the response to part (a), growth fault GM-K is interpreted to not offset horizons 3 and 4 in the seismic lines and does not deform the surface. Based on these observations of a lack of deformation and the distance between the surface projections and the power block area, there is no potential for growth fault GM-K to deform the surface within the power block area.

Associated ESPA Revision:

No ESPA revision is required as a result of this response.

ATTACHMENT 9

SUMMARY OF REGULATORY COMMITMENTS

(Exelon Letter to USNRC, NP-11-0027, dated June 28, 2011)

The following table identifies commitments made in this document. (Any other actions discussed in the submittal represent intended or planned actions. They are described to the NRC for the NRC's information and are not regulatory commitments.)

COMMITMENT	COMMITTED DATE	COMMITMENT TYPE	
		ONE-TIME ACTION (Yes/No)	Programmatic (Yes/No)
Exelon will revise the VCS ESPA SSAR Section 2.5.1 to incorporate the change shown in the enclosed response to the following NRC RAI: 02.05.01-10 (Attachment 5)	Revision 1 of the ESPA SSAR and ER planned for no later than March 31, 2012	Yes	No